Geological Magazine

www.cambridge.org/geo

Original Article

Cite this article: Batkhuyag E, Tserendash N, Tumen-Ulzii O, Tong Y, Lei G, Khurelbaatar U, and Garvaa B. U-Pb ages and Hf isotope data from detrital zircons in the metasedimentary rocks of the Mongolian Altai Group, Mongolian part of the Altai-Mongolian Terrane: implications on the provenance and tectonic setting. *Geological Magazine* **161**(e27): 1–36. https://doi.org/10.1017/S0016756824000529

Received: 27 April 2024
Revised: 30 October 2024
Accepted: 17 November 2024

Keywords:
detrital zircon; depositional timing; Mongolian Altai; tectonic evolution

Corresponding author:
Enkhdalai Batkhuyag;
Email: enkhdalaib@mas.ac.mn

U-Pb ages and Hf isotope data from detrital zircons in the metasedimentary rocks of the Mongolian Altai Group, Mongolian part of the Altai-Mongolian Terrane: implications on the provenance and tectonic setting

Enkhdalai Batkhuyag[1,2], Narantsetseg Tserendash[1], Oyunchimeg Tumen-Ulzii[1], Ying Tong[3], Guo Lei[3], Udaanjargal Khurelbaatar[4] and Batzorig Garvaa[4]

[1]Institute of Geology, Mongolian Academy of Sciences, Ulaanbaatar 15160, Mongolia; [2]School of Geology and Mining Engineering, MUST, Ulaanbaatar 14191, Mongolia; [3]Institute of Geology, Chinese Academy of Geological Sciences, 100037 Beijing, China and [4]Ereenchuluu LLC, Ulaanbaatar 14200, Mongolia

Abstract

In this paper, we present the new results of the U–Pb age dating and Lu-Hf isotopic analysis of detrital zircons of the four representative metasedimentary rock samples from the Mongol Altai Group, Mongolian part of the Altai-Mongolian terrane. Our new results indicate that the metasedimentary rocks of the Mongol Altai Group were formed after ~497 Ma, Late Cambrian and deposited during the Early-Middle Ordovician. The detrital zircons of four samples yield a two major age peaks at 503–517 Ma, and 775–843 Ma, respectively, with minor involvement of older zircons. The nearby Lake Zone of Ikh-Mongol Arc most likely provided plenty of Early Paleozoic materials, the subdominant Neoproterozoic detrital zircons could be supplied by the felsic intrusions along the western margin of the Tuva-Mongol microcontinent, and the sparse older zircons may be derived from its basement. With combination of previous studies in the Chinese Altai, Russian Altai and Hovd terrane, our data suggest that the Altai–Mongolian terrane possibly represents a coherent continental arc-accretionary prism system built upon the active margin of the western Mongolia during the Cambrian to Ordovician. Moreover, the dominant Neoproterozoic to Early Paleozoic detrital zircons from the Mongol Altai sequence yield largely varied εHf(t) values from −17.4 to +12.0, indicating that input juvenile material and reworking of crustal components are both important in the accretionary orogenesis. A compilation of U–Pb and Hf isotope data of detrital zircons shows that the source area underwent two most extensive magmatic activities at ca. 470–574 Ma and 687–967 Ma, respectively.

1. Introduction

The Central Asian Orogenic Belt (CAOB) is one of the largest accretionary orogens worldwide, formed from Neoproterozoic to Mesozoic times by continuous accretion of various terranes (Şengör *et al.* 1993; Windley *et al.* 2007). It can be subdivided into two main parts: the eastern Mongolian and western Kazakhstan collage systems, which consist of Precambrian ribbon continents and Late Proterozoic to Early Paleozoic arcs, back-arcs and accretionary complexes (Şengör & Natal'in, 1996; Xiao *et al.* 2018). These vast orogenic systems are limited in the south by a collage of amalgamated small continental blocks, Paleozoic arcs and accretionary complexes north of the Tarim and North China cratons (Fig. 1).

The Altai-Mongolian terrane, one of the representative tectonic units in the Mongolian collage, plays an important role in reconstructing the evolution history of the CAOB. This ~1000 km long and up to 250 km wide terrane or microcontinent extends southwards from the Russian Altai in Siberia, via the Mongolian Altai in Mongolia, to the Chinese Altai in China (Windley *et al.* 2007; Chen *et al.* 2014).

The Chinese Altai comprises mainly Cambrian to Silurian turbiditic and pyroclastic/volcanic sequence (Habahe and Kulumuti groups), and Devonian to Carboniferous low-grade metasedimentary and metavolcanic rocks (Windley *et al.* 2002; Long *et al.* 2007, 2008; Sun *et al.* 2008, 2009; Cai *et al.* 2011a). The Russian Altai consists of mainly thick middle Cambrian to early Ordovician greenschist-facies metasandstones and meta-siltstones, and transgressively overlying by middle Ordovician to early Silurian marine sediments and Devonian volcaniclastic sedimentary rocks (Buslov *et al.* 2001; Daukeev *et al.* 2008; Chen *et al.* 2014a, 2014b, 2015, 2016). The intrusive rocks in the Russian and Chinese Altai are dominated by early–middle Paleozoic

https://doi.org/10.1017/S0016756824000529 Published online by Cambridge University Press

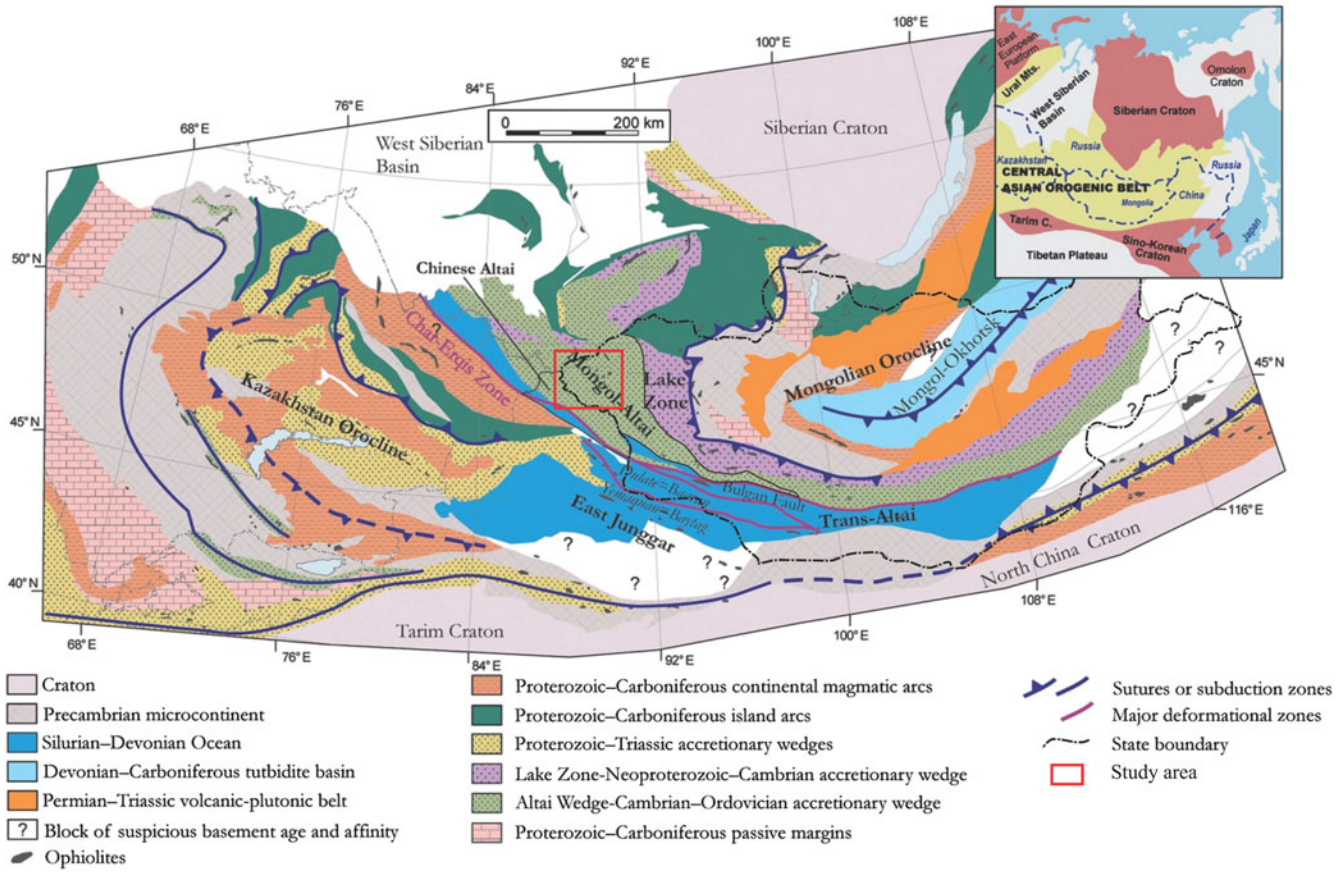

Figure 1. Tectonic map of the Mongolian collage system and the adjacent Kazakhstan collage constituting the central part of the CAOB (modified from Sengör *et al.*, 1993; Kröner *et al.*, 2010; Guy *et al.*, 2020).

and minor late Paleozoic to Mesozoic granitic plutons (Windley *et al.* 2002; Wang *et al.* 2006; Yuan *et al.* 2007; Sun *et al.* 2008; Cai *et al.* 2011b; Glorie *et al.* 2011).

The Altai-Mongolian terrane was previously considered a Precambrian microcontinent based on some old whole-rock Sr-Nd isotopic data of supracrustal rocks exposed in the Russian and Chinese Altai (Mossakovsky *et al.* 1994; Dobretsov *et al.* 1995; Hu *et al.* 2000; Buslov *et al.* 2001; Windley *et al.* 2002; Li *et al.* 2006; Yang *et al.* 2011). However, some geochronological studies revealed that the gneissic granitic rocks in the Chinese Altai were actually formed in ca. 480–450 Ma (Wang *et al.* 2006; Briggs *et al.* 2007; Sun *et al.* 2008; Cai *et al.* 2011*b*) and thus do not support a Precambrian origin.

The geochronological studies from Chinese Altai show that these low-grade flysch-like sedimentary sequences, which grouped into the Habahe Group and their high-grade metamorphic equivalent-paragneiss, were deposited in an active continental margin or a continental arc setting prior to the Middle Ordovician in the Eastern Chinese Altai and between the Early Silurian and Early Devonian in the north-western Chinese Altai (Long *et al.* 2007, 2008, 2010; Jiang *et al.* 2011). The provenance of the metasedimentary rocks in the Chinese Altai was dominated by Cambrian to Early Ordovician igneous rocks, with subordinate Neoproterozoic and minor Paleoproterozoic and Archean crustal materials (Long *et al.* 2007, 2008, 2010). Moreover, the recent study shows that the meta-sedimentary sequences in the southern part of Russian Altai were deposited in the Early–Middle Ordovician in an active continental margin, with sediment sources mainly from the Neoproterozoic to Early Paleozoic magmatic rocks in the Tuva-Mongolian block and adjacent island arcs in western Mongolia in the Early Paleozoic (Chen *et al.* 2014). A similar conclusion has also been made for the high-grade paragneisses in the Tseel terrane southeastern extension of the Chinese Altai in western Mongolia (Jiang *et al.* 2012). Synthesizing all data from the Russian and Chinese Altai and Tseel terranes, arc-accretionary prism was built upon the active margin of western Mongolia in the Early Paleozoic (Jiang *et al.* 2017).

In the Mongolian part of the Altai-Mongolian terrane, Early Paleozoic flysch deposits are widely distributed and grouped into the 'Mongolian Altai Group' (Tomurtogoo *et al.* 1998). Although the lithological characters of the Mongolian Altai Group are quite similar to those of Chinese Altai and Russian Altai, the depositional age, provenance and tectonic setting are poorly constrained and still under debate.

The Mongolian Altai Group was originally assigned a Middle Cambrian-Early Ordovician (Dergunov *et al.*, 1980; 2001; Tomurtogoo *et al.* 1998), but some workers favoured Cambrian or Middle-Upper Cambrian ages (Badarch *et al.* 2002; Tovuudorj & Sumya, 2008; Erdenechimeg *et al.* 2018) without precise geochronological data. High-resolution geochronological data were reported by Long *et al.* (2019) Sukhbaatar *et al.* (2022) and Soejono *et al.* (2018) only from the southern and western parts of the Mongolian Altai. Based on the detrital zircon U-Pb age dating of five metasedimentary rocks, these authors proposed that the sedimentary sequence in the southern part of Mongolian Altai was deposited during the Late Silurian and Early Devonian on an active continental margin, which is consistent with the Habahe group in

https://doi.org/10.1017/S0016756824000529 Published online by Cambridge University Press

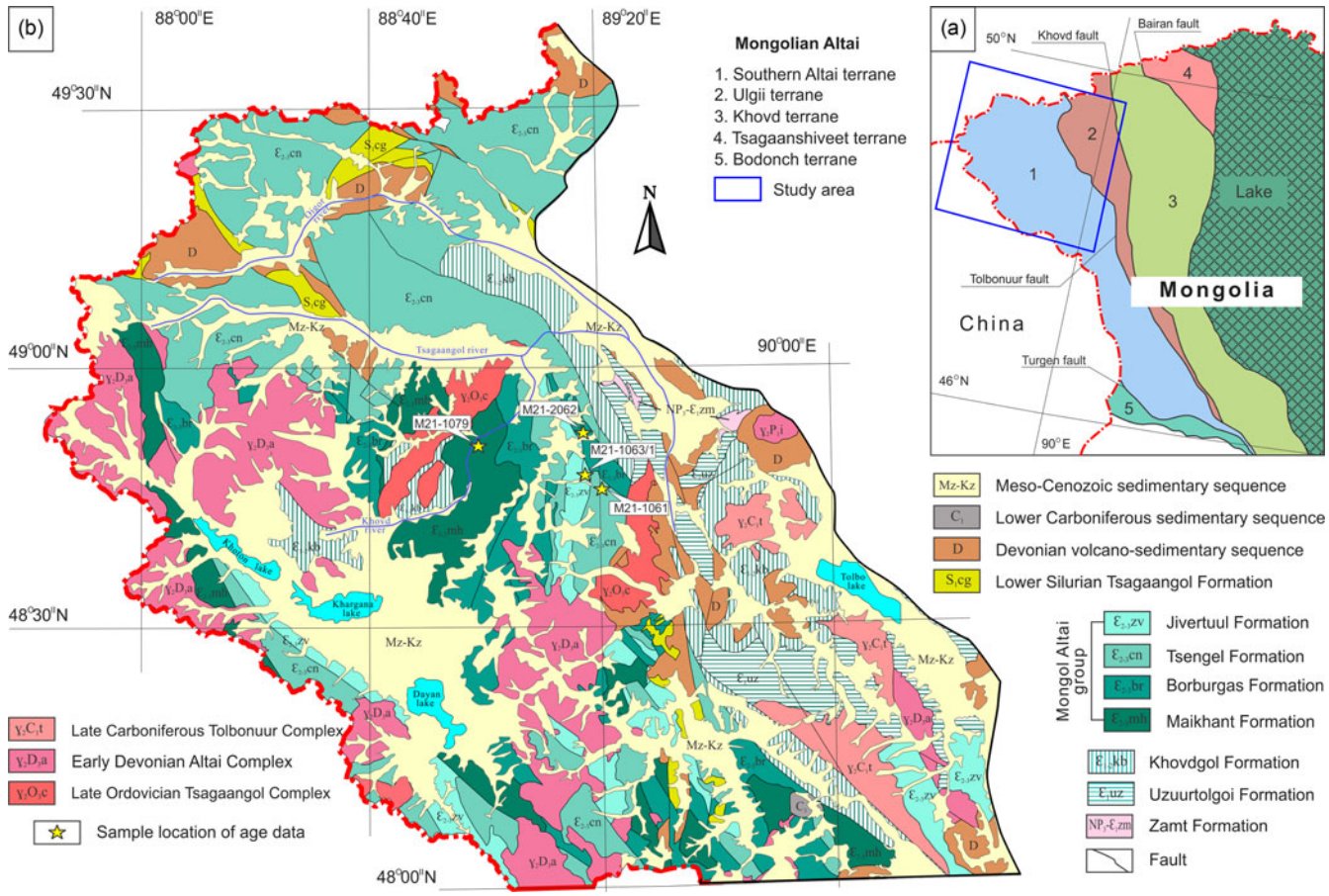

Figure 2. (a) The tectonic map of Mongolia (Tomurtogoo, 2014), showing the location of the Mongolian Altai Orogenic System. (b) Simplified geological map of the Southern Altai terrane (modified after Tovuudorj & Sumya, 2008).

the western Chinese Altai (Long *et al.* 2007, 2010, 2012; Dong *et al.* 2018). However, this conclusion cannot be used for the whole Mongolian Altai without studying the northern part, where almost all key sections of the Mongolian Altai Group were reported.

Therefore, in order to fill this gap, we have conducted detailed field investigations and sampling for geochronological and geochemical analyses of the metasedimentary sequences of the Mongolian Altai Group exposed in the northern part of the Mongolian Altai. In this paper, we present the new results of the U-Pb age dating and Lu-Hf isotopic analysis of detrital zircons from the metasedimentary rocks of the Mongolian Altai Group with the aim of constraining the depositional ages, provenances and tectonic setting in order to reconstruct the Early Paleozoic evolution of the orogenic belt.

2. Geology of the study area

The Mongolian Altai or so-called Mongolian Altai Fold System (Tomurtogoo, 2014, 2017), located in western Mongolia, extends to the west and north into China, Kazakhstan and Russia (Dergunov *et al.* 1980; Dobretsov *et al.* 1995; Badarch *et al.* 2002; Tomurtogoo, 2002; Tomurtogoo, 2012, 2014; 2017). According to the latest tectonic subdivision of Mongolia, the Mongolian Altai is structurally subdivided into five major tectonic units, namely the Southern Altai, Ulgii, Khovd, Tsagaanshiveet and Bodonch terranes, which converged probably in the Early Ordovician (Tomurtogoo, 2014). The Tolbonuur Fault defines the boundary between Southern Altai and Ulgii terranes, while the Khovd and Bairam Faults constitute the boundary between Ulgii/Khovd and Khovd/Tsagaanshiveet terranes, respectively (Fig. 2a). The Southern Altai Terrane (Altai Terrane by Badarch *et al.* 2002) makes up the most extreme southwest high-altitude part of the Mongolian Altai Range. According to the State Geological Map with 1:200000 scale, the terrane consists of basalt, mafic tuff, limestone of the Upper Neoproterozoic–Lower Cambrian Zamt Formation (NP_3–$Є_1$zm), quartzite, metasandstone and metasiltstone of the Lower Cambrian Uzuurtolgoi Formation ($Є_1$uz), calcareous and siliceous metasandstone, metasiltstone and minor metaconglomerate of the Lower-Middle Cambrian Khovdgol Formation ($Є_{1\text{-}2}$kb), and thick monotonous terrigenous sandstone-siltstone of the Middle-Upper Cambrian Mongolian Altai Group (Tovuudorj *et al.* 2008) (Fig. 2b).

The terrane is overlain by Silurian, Devonian and minor Lower Carboniferous shallow-marine sedimentary and volcanic rocks and intruded by Upper Ordovician, Early Devonian and Upper Carboniferous granite plutons (Fig. 2b). Among them, sandstone-siltstone series rocks of the Mongolian Altai Group are characterized by wide distribution and are usually compared with the 'Gorny-Altai' series, determined in the adjacent area of the Russian Altai (Dergunov *et al.* 1980; Chen *et al.* 2014, 2016) and with the Habahe Group in the Chinese Altai (Sun *et al.* 2008; Long *et al.* 2007, 2008, 2010; Jiang *et al.* 2012).

The Mongolian Altai Group extensively outcrops in the northern part of the Mongolian Altai and is stratigraphically divided into the Maikhant ($Є_{2\text{-}3}$mh), Borburgas ($Є_{2\text{-}3}$br), Tsengel

https://doi.org/10.1017/S0016756824000529 Published online by Cambridge University Press

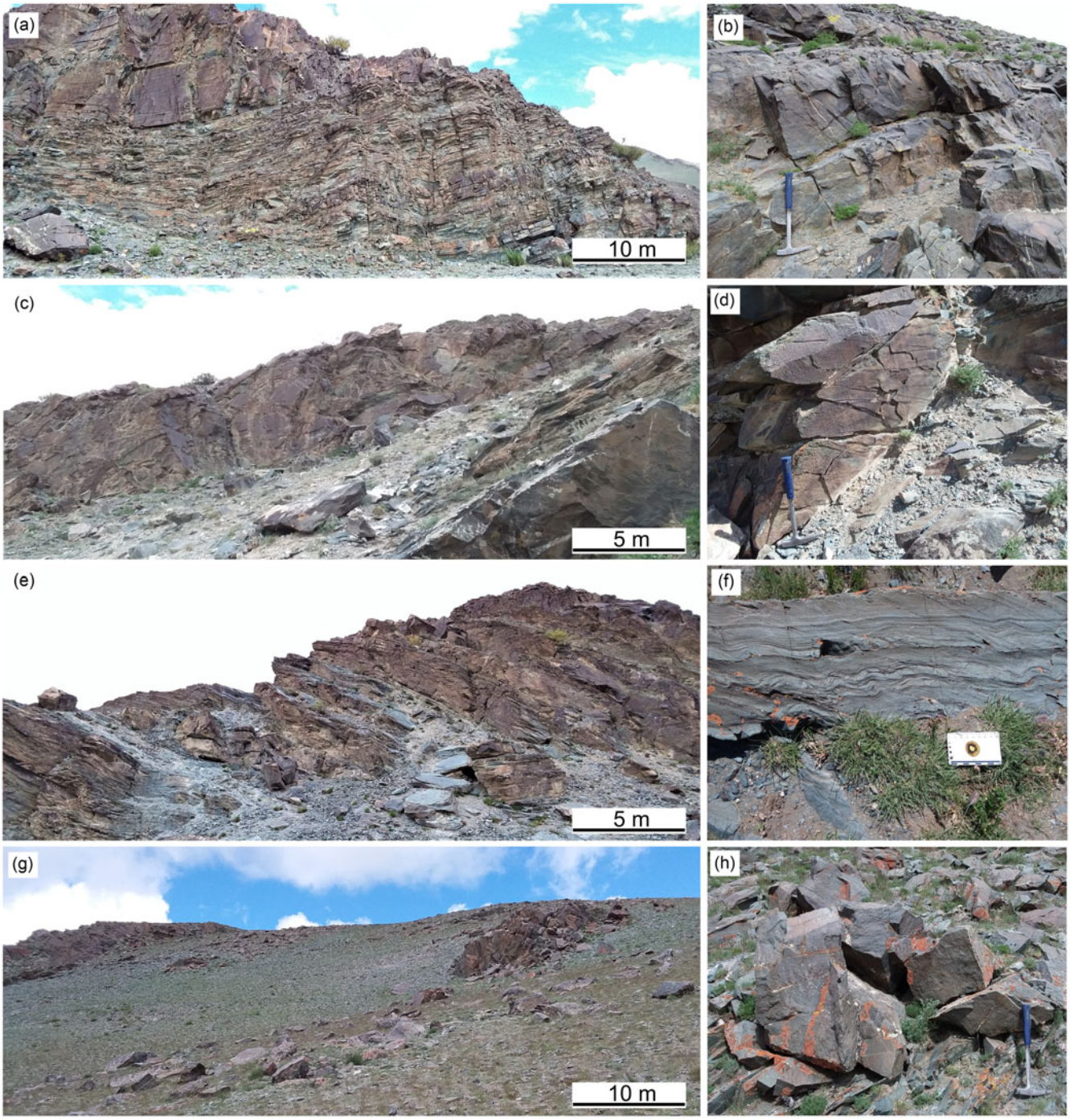

Figure 3. Field photographs showing constituent metasedimentary rocks from the Mongolian Altai Group, northern part of the Altai terrane, Western Mongolia. (a, b) fine- to medium-grained quartz metasandstone, metasiltstone (Maikhant Formation). (c, d) fine to medium-grained feldspar-quartz sandstone and metasiltstone (Borburgas Formation). (e, f) liliaceous siltstone with interlayers of sandstone (Tsengel Formation). (g, h) medium- to coarse-grained sandstone, and siltstone (Jivert-Uul Formation).

($\mathcal{E}_{2\text{-}3}$cn) and Jivert-Uul ($\mathcal{E}_{2\text{-}3}$zv) Formations from bottom to top based on geological correlation (Fig. 2b).

The Maikhant Formation is well exposed along the left and right banks of the River Khovd and Bor Us, Khoton Khargai, Serge Zurkh, Khovd and Bayanzurkh Mountains. According to the field observation, the Maikhant Formation is composed mainly of intercalation of greenish grey and greenish fine- to medium-grained metasandstone, metasiltstone, schist and minor calcareous sandstone, and liliaceous metasiltstone (Figs. 3a and b). The sediments are scrutinized by numerous discontinuous faults, generally dipping 30–50° to the northeast, and occur as monoclinal structures.

The Borburgas Formation is characterized by lesser distribution and studied along the right bank of the River Khovd, the southern part of the Ikh-Khar Lake, Gurvan Khairkhant and the Tashint Mountains area. The formation consists of an alternation of greenish and greenish-grey fine to medium-grained feldspar-quartz sandstone, quartz sandstone and metasiltstone, minor schist and lens of metaconglomerate (Figs. 3c and d). The

https://doi.org/10.1017/S0016756824000529 Published online by Cambridge University Press

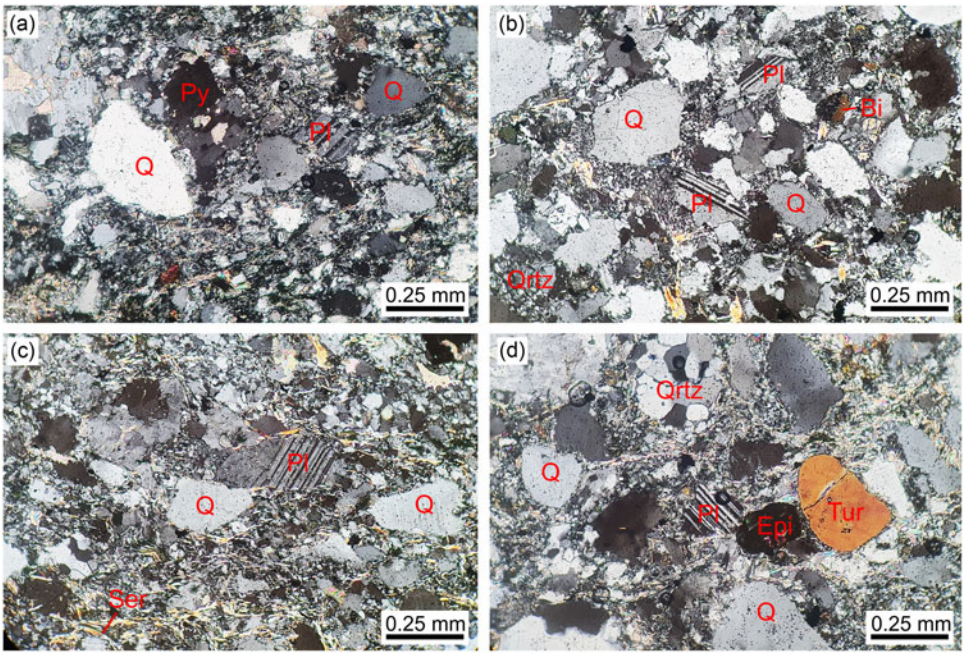

Figure 4. Representative photomicrographs of the samples used for detrital zircon U-Pb geochronology. (a) Medium-grained metasandstone sample M21-1079/1; (b) Medium-grained metasandstone (sample M21-2062); (c) Medium-grained schistose sandstone (sample M21-1061); (d) Medium-coarse-grained metasandstone (sample M21-1063/1). Legend: Q-quartz, Pl-plagioclase, Epi-epidote, Tur-tourmaline, Py-pyrite, Bi-biotite, Ser-sericite, rock fragments: Qrtz-quartzite.

formation is bounded by a northwest-oriented tectonic fault with sedimentary rocks from the Maikhant and Tsengel formations. The sediment is dipping 35–40° to the east and southeast.

The Tsengel Formation is studied along the right and left banks of the Rivers Khargant, Khatuu, Tsagaan and Nuraat Mountain. The formation in these areas consists of greenish to liliaceous siltstone with interlayers of sandstone and a minor conglomerate lens (Figs. 3e and f). The siltstone has a rhythmic-bedded structure and is micro-folded. The sediment is dipping 40–60° to the northwest and is cut by granites of the Late Devonian Altai Complex.

The uppermost Jivert-Uul Formation is studied around the Balgant Mountain area. In this area, about 300 m-thick greenish grey and greenish medium- to coarse-grained sandstone inter-bedded with siltstone belong to the Mongolian Altai Group (Figs. 3g and h). Lithology of succession is quite identical to those of the Tsengel and other Formations from Mongolian Altai Group. They have undergone intense horizontal compression and folding, and have been crosscut by 0.1–0.5 cm late-stage quartz veins, with displacement along faults.

A total of seventy metasedimentary samples were collected from a Paleozoic sequence in the northern part of the Altai terrane, Western Mongolia (Fig. 2b). Among these samples, four were prepared for detrital zircon U-Pb dating and Lu-Hf isotopic analysis.

3. Sample locations and descriptions

Based on detailed geological field work, we selected four representative samples from the metasedimentary strata, which are mapped as the Middle-Upper Cambrian Maikhant, Borburgas, Tsengel and Jivert-Uul Formations of the Mongolian Altai Group, respectively, for detrital zircon U-Pb dating and Lu-Hf isotopic analysis. Sample locations are shown in Figure 2b, and a short description of the rocks is given below.

3.a. Metasandstone sample M21-1079/1

Sample M21-1079/1 was collected from the north-western part of the Gurvan Khairgant Mountain, right bank of the Khovd River (GPS location: 48° 50′ 49.7″ N; 88° 59′ 42″ E). It is a greenish-grey, medium-grained metasandstone with a psammitic structure, belonging to the Maikhant Formation. The rock consists of quartz 30–35 vol.%, feldspar (10–15 vol.%), epidote (5 vol.%), biotite and muscovite (5 vol.%) and lithic fragments (10–15 vol.%) in a fine-grained matrix of quartz, chlorite and sericite (30–35 vol.%). The grains tend to be moderately well-rounded and moderately sorted. Lithic fragments are quartzite and schists in composition (Fig. 4a).

3.b. Metasandstone sample M21-2062

Sample M21-2062 was collected from the south-eastern part of the Ust Uzuur Mountain (GPS location: 48° 51′ 7.7″ N; 89° 16′ 45.4″ E). It is a medium-grained metasandstone belonging to the Borburgas Formation. The metasandstone is psammitic in structure and moderately sorted and consists of sub-rounded and rounded clasts of quartz 30–35 vol.%, feldspar (15–20 vol.%), epidote (5–10 vol.%), opaque mineral (5–10 vol.%), minor biotite and lithic fragment (10–15 vol.%) in a fine-grained matrix of quartz, chlorite, sericite and clayey materials (15–20 vol.%) (Fig. 4b).

3.c. Metasandstone sample M21-1061

Sample M21-1061 is a medium-grained metasandstone from the Tsengel Formation, collected north-eastern part of the Jivert Mountain (GPS location: 48° 46′ 0.2″ N; 89° 18′ 43.8″ E). The metasandstone is moderately sorted and slightly metamorphosed, which is represented by schistose structure. The sample consists of moderately rounded clasts of quartz 10–15 vol.%, feldspar (25–30 vol.%), carbonate (5 vol.%), minor amphibole (hornblende) and lithic fragments (15–20 vol.%) in a fine-grained matrix of quartz, chlorite and sericite (35–40 vol.%). Accessory mineral is represented by zircon grains (Fig. 4c).

3.d. Metasandstone sample M21-1063/1

Sample M21-1063/1 is a metasandstone from the strata, which was mapped as the Jivert-Uul Formation. A sample was taken from the south-eastern part of the Balgant Mountain (GPS location:

https://doi.org/10.1017/S0016756824000529 Published online by Cambridge University Press

48° 46′ 43.3″ N; 89° 17′ 8.4″ E). The metasandstone is psammitic in structure and moderately sorted and consists of moderately well-rounded quartz 40–45 vol.%, feldspar (10–15 vol.%), epidote (5–10 vol.%), minor tourmaline, opaque minerals and lithic fragment (15–20 vol.%) in a fine-grained matrix of quartz, chlorite, sericite and clayey materials (15–20 vol.%) (Fig. 4d).

4. Analytical methods

Rock samples were crushed in a steel jaw crusher. A shaking bed and heavy liquid techniques were used to separate heavy minerals. Zircon grains from the heavy mineral fraction by hand-picking under a binocular microscope. About 300 grains were selected from each sample and mounted on adhesive tape, then enclosed in epoxy resin and polished to about half of their diameter. After being photographed under reflected and transmitted light, the samples were prepared for cathodoluminescence (CL) imaging, U-Pb dating and Hf isotope analysis.

4.a. Zircon CL imaging and U-Pb dating

Prior to analysis, CL imaging of the zircons was performed using an FEI PHILIPS XL30 SFEG instrument with a 2-min scanning time at 15 kV and 120 nA at the Beijing SHRIMP Center, Chinese Academy of Geological Sciences (CAGS), Beijing, China.

U-Pb dating of zircon was conducted by laser ablation inductively coupled plasma mass spectrometry (LA-ICP-MS) at the Sincere spectrum Detection Technology (Langfang) Co., Ltd., China. Experiments were carried out on the Analytik Jena AG PQMS030 elite ICP-MS instrument (Germany) in combination with an excimer 193 nm laser ablation system (NewWave, NWR193). All LA-ICP-MS measurements were carried out using time-resolved analysis in fast, peak jumping mode. Each spot analysis consisted of approximately 30s background acquisition followed by 30s data acquisition from the sample. The excimer laser system is equipped with apertures, which image the laser beam onto the sample surface. This optical configuration allows the selection of a constant fluence that is independent of crater diameters. Helium was used as a carrier gas. Details of the instrumental operating conditions and measurement parameters are reported in Tables 1 to 4.

The spot size and frequency of the laser were set to 35 μm and 13Hz, respectively, in this study. NIST SRM610 was used to yield the highest sensitivity, the lowest oxidation and background and a stable signal to achieve optimal conditions. Setting a 15-ms dwell time for ^{204}Pb, ^{206}Pb, ^{207}Pb ^{208}Pb, ^{232}Th and ^{238}U. Zircon Plesovice (Sláma *et al.* 2008) and Qinghu (Li *et al.* 2013) were used as external standards for U-Pb dating and blind samples for monitoring the instrument condition, respectively, and were measured twice every five samples analyzed. Approximately 30 seconds of background data acquisition were conducted for each analysis. Data reduction was made using GLITTER 4.0 software (Macquarie University) and plotted by Isoplot 4.15 (Ludwig, 2003). Concentration values of NIST SRM 610 used for external calibration were taken from (Pearce, 1997).

4.b. Hf isotope analysis

Zircon Lu-Hf isotope analyses were performed using a Newwave UP213 laser ablation microprobe attached to a Neptune multi-collector ICP-MS at the Institute of Mineral Resources, CAGS, Beijing. The instrumental conditions and data acquisition follow those described by Hou *et al.* (2007). A stationary spot with a beam diameter of either 40 μm or 55 μm was used, depending on the size of the ablated domains. The gas, in combination with Ar, was used as the carrier gas to transport the ablated sample from the laser ablation cell to the ICP-MS torch via a mixing chamber. To correct for the isobaric interferences of ^{176}Lu and ^{176}Yb with ^{176}Hf, ^{176}Lu/^{175}Lu = 0.02658 and ^{176}Yb/^{173}Yb = 0.796218 ratios were determined (Chu *et al.* 2002). For instrumental mass bias corrections, Yb isotope ratios were normalized to a ^{172}Yb/^{173}Yb ratio of 1.35274 (Chu *et al.* 2002) and Hf isotope ratios to a ^{179}Hf/^{177}Hf ratio of 0.7325 using an exponential law. The mass-bias behaviour of Lu was assumed to follow that of Yb. The mass bias correction protocols were performed as described by Hou *et al.* (2007). The zircon GJ1 was used as the reference standard, with a weighted mean ^{176}Hf/^{177}Hf ratio of 0.282008 ± 27 (2σ) during our routine analyses. This ratio is not distinguishable from a weighted mean ^{176}Hf/^{177}Hf ratio of 0.282013 ± 19 (2σ), according to in situ analysis by Elhlou *et al.* (2006). The calculation of the Hf model age (single-stage model age; T_{DM}) is based on a depleted-mantle source with a modern ^{176}Hf/^{177}Hf ratio of 0.28325 and the ^{176}Lu decay constant of 1.865×10^{-11} year^{-1} (Scherer *et al.* 2001). The calculation of the 'crust' (two-stage) Hf model age (T_{DM}^{C}) is based on the assumption of a mean ^{176}Lu/^{177}Hf value of 0.011 for average continental crust (Wedepohl, 1995). The calculation of εHf(t) values was based on zircon U-Pb ages and chondritic values (^{176}Hf/^{177}Hf = 0.282772, ^{176}Lu/^{177}Hf = 0.0332; Blichert-Toft & Albarede, 1997).

5. Results

The U-Pb ages and Hf isotope compositions of the zircons from four analyzed metasandstone samples are given in Tables 1 to 5, respectively.

5.a. Metasandstone from the Maikhant formation (Sample M21-1079/1)

A total of one hundred and ten zircon grains were analyzed. Zircons from sample M21-1079/1 are colourless, with euhedral to subhedral shapes. They range in length from ca. 80 to 150 μm, with length-to-width ratios of 1.5:1 to 3:1. In CL images, most grains display oscillatory growth zoning, indicating a magmatic origin, whereas the few rims are overgrowth formed during the migmatization (Hanchar & Hoskin, 2003) (Fig. 5a).

The Th/U ratios of zircons vary between 0.1 and 1.2 (except for M21-1079_77, 36, 90 < 0.1). The high Th/U ratios of zircons (>0.1) and observed oscillatory growth zoning in CL images suggest that the most detrital zircons were derived from a magmatic provenance (Koschek, 1993).

From one hundred and ten analyses performed in the metasandstone M21-1079/1, ninety-seven yield concordant ages ranging from 470 ± 10 to 1970 ± 39 Ma (Fig. 6a). The obtained ages are mainly clustering at 470–530 Ma, 744–967 Ma and 1944–1970 Ma, with the prominent age peak at 509 Ma (n = 74; 76 %), 775 Ma (n = 17; 18 %), and minor peaks at 1589 Ma (n = 4; 4 %), and 1959 Ma (n = 2; 2 %), respectively (Fig. 6b). The youngest coeval zircon grains between 470 ± 10 and 485 ± 11 Ma yield a weighted mean age of 474.0 ± 6.1 Ma (MSWD = 1.49, n = 10) (Fig. 6c).

Sixteen representative zircons were analyzed for Hf isotope compositions. Twelve Cambrian and Ordovician zircons give ^{176}Hf/^{177}Hf values varying from 0.281975 to 0.282671. The εHf(t) value and T_{DM}^{C} model ages range from −17.4 to +4.9 and from 1.0–2.5 Ga, respectively. Other two Neoproterozoic zircons have

https://doi.org/10.1017/S0016756824000529 Published online by Cambridge University Press

Table 1. U–Pb data for zircons from metasandstone in the Maikhant Formation (Sample M21-1079/1)

Analysis		Corrected ratios						Corrected ages (Ma)						
	Th/U ratios	$^{207}Pb/^{206}Pb$	1σ	$^{207}Pb/^{235}U$	1σ	$^{206}Pb/^{238}U$	1σ	$^{207}Pb/^{206}Pb$	1σ	$^{207}Pb/^{235}U$	1σ	$^{206}Pb/^{238}U$	1σ	Disc %
M21-1079-01	0.76	0.05472	0.00183	0.62245	0.02127	0.08260	0.00182	400	73	491	13	512	11	-4
M21-1079-02	0.45	0.05856	0.00143	0.66662	0.01708	0.08265	0.00179	551	52	519	10	512	11	1
M21-1079-03	1.15	0.12106	0.00266	5.93230	0.13912	0.35580	0.00770	1972	39	1966	20	1962	37	0
M21-1079-04	1.25	0.06713	0.00229	1.16213	0.04040	0.12570	0.00278	842	69	783	19	763	16	3
M21-1079-05	0.10	0.07207	0.00167	1.47363	0.03615	0.14847	0.00322	988	47	920	15	892	18	3
M21-1079-06	0.97	0.05639	0.00138	0.64113	0.01649	0.08256	0.00179	467	54	503	10	511	11	-2
M21-1079-07	0.80	0.06586	0.00152	0.66630	0.01623	0.07346	0.00159	802	47	519	10	457	10	13
M21-1079-08	0.13	0.06241	0.00141	0.71012	0.01709	0.08261	0.00179	688	48	545	10	512	11	6
M21-1079-09	0.73	0.06471	0.00170	0.72551	0.01988	0.08141	0.00178	765	55	554	12	505	11	10
M21-1079-10	0.94	0.06579	0.00210	0.72734	0.02383	0.08027	0.00176	800	65	555	14	498	10	12
M21-1079-11	0.73	0.06364	0.00187	0.68532	0.02073	0.07819	0.00172	730	61	530	12	485	10	9
M21-1079-12	0.44	0.05643	0.00129	0.61958	0.01506	0.07972	0.00172	469	50	490	9	494	10	-1
M21-1079-13	0.94	0.05714	0.00144	0.64590	0.01708	0.08208	0.00178	496	55	506	11	509	11	0
M21-1079-14	0.90	0.06012	0.00144	0.64422	0.01622	0.07781	0.00169	608	51	505	10	483	10	5
M21-1079-15	1.09	0.06399	0.00178	1.13686	0.03281	0.12899	0.00283	741	58	771	16	782	16	-1
M21-1079-16	0.43	0.05658	0.00137	0.64461	0.01640	0.08272	0.00179	475	53	505	10	512	11	-1
M21-1079-17	0.44	0.06117	0.00165	0.68806	0.01924	0.08167	0.00179	645	57	532	12	506	11	5
M21-1079-18	0.68	0.06433	0.00165	0.72472	0.01951	0.08179	0.00177	753	53	553	11	507	11	9
M21-1079-19	1.02	0.06650	0.00221	1.20288	0.04060	0.13134	0.00294	822	68	802	19	796	17	1
M21-1079-20	0.66	0.06746	0.00184	1.21882	0.03449	0.13119	0.00285	852	56	809	16	795	16	2
M21-1079-21	0.77	0.05708	0.00141	0.65456	0.01697	0.08327	0.00181	494	54	511	10	516	11	-1
M21-1079-22	0.16	0.06679	0.00148	0.76392	0.01801	0.08304	0.00179	831	45	576	10	514	11	12
M21-1079-23	0.67	0.06698	0.00176	0.76442	0.02088	0.08286	0.00181	837	54	577	12	513	11	12
M21-1079-24	0.36	0.08464	0.00185	2.56189	0.05990	0.21977	0.00474	1307	42	1290	17	1281	25	1
M21-1079-25	0.72	0.05973	0.00164	0.63108	0.01796	0.07672	0.00168	594	58	497	11	477	10	4
M21-1079-26	0.74	0.05622	0.00208	0.61744	0.02318	0.07974	0.00177	460	80	488	15	495	11	-1
M21-1079-27	0.14	0.07218	0.00166	1.57723	0.03849	0.15866	0.00343	991	46	961	15	949	19	1
M21-1079-28	0.16	0.06997	0.00151	1.25717	0.02911	0.13046	0.00281	927	44	827	13	791	16	5
M21-1079-29	0.34	0.05410	0.00125	0.60687	0.01488	0.08146	0.00176	375	51	482	9	505	10	-5
M21-1079-30	0.33	0.06268	0.00142	0.70117	0.01687	0.08123	0.00176	697	48	540	10	503	10	7

(*Continued*)

Table 1. (*Continued*)

Analysis		Corrected ratios						Corrected ages (Ma)						
	Th/U ratios	$^{207}Pb/^{206}Pb$	1σ	$^{207}Pb/^{235}U$	1σ	$^{206}Pb/^{238}U$	1σ	$^{207}Pb/^{206}Pb$	1σ	$^{207}Pb/^{235}U$	1σ	$^{206}Pb/^{238}U$	1σ	Disc %
M21-1079-31	0.57	0.06307	0.00265	0.72538	0.03072	0.08351	0.00187	711	87	554	18	517	11	7
M21-1079-32	0.30	0.06296	0.00139	0.71608	0.01681	0.08258	0.00178	707	46	548	10	512	11	7
M21-1079-33	0.12	0.06364	0.00136	0.72699	0.01669	0.08295	0.00179	730	45	555	10	514	11	8
M21-1079-34	0.81	0.06457	0.00189	0.73703	0.02217	0.08288	0.00182	760	60	561	13	513	11	9
M21-1079-35	0.22	0.05840	0.00127	0.66892	0.01554	0.08316	0.00179	545	47	520	9	515	11	1
M21-1079-36	0.06	0.07090	0.00154	1.51482	0.03518	0.15513	0.00334	955	44	936	14	930	19	1
M21-1079-37	0.20	0.06132	0.00132	0.70472	0.01621	0.08344	0.00180	651	45	542	10	517	11	5
M21-1079-38	0.53	0.06412	0.00182	0.73415	0.02149	0.08313	0.00182	746	59	559	13	515	11	9
M21-1079-39	1.02	0.06593	0.00149	1.17008	0.02807	0.12886	0.00278	804	47	787	13	781	16	1
M21-1079-40	0.56	0.06510	0.00147	0.71395	0.01714	0.07963	0.00172	778	47	547	10	494	10	11
M21-1079-41	0.75	0.12051	0.00351	5.84410	0.17513	0.35210	0.00784	1964	51	1953	26	1945	37	0
M21-1079-42	0.73	0.05380	0.00288	0.61614	0.03284	0.08315	0.00197	363	116	487	21	515	12	-5
M21-1079-43	0.47	0.06065	0.00134	0.69517	0.01637	0.08322	0.00180	627	47	536	10	515	11	4
M21-1079-44	0.51	0.05971	0.00157	0.68339	0.01874	0.08310	0.00181	594	56	529	11	515	11	3
M21-1079-45	0.13	0.06702	0.00146	0.78230	0.01818	0.08475	0.00183	839	45	587	10	524	11	12
M21-1079-46	0.24	0.05564	0.00186	0.61341	0.02095	0.08005	0.00176	438	73	486	13	496	10	-2
M21-1079-47	0.67	0.06749	0.00151	0.75557	0.01800	0.08129	0.00176	853	46	572	10	504	10	13
M21-1079-48	0.97	0.06725	0.00228	1.20946	0.04172	0.13058	0.00292	846	69	805	19	791	17	2
M21-1079-49	0.71	0.06402	0.00159	1.10201	0.02877	0.12498	0.00271	742	52	754	14	759	16	-1
M21-1079-50	0.41	0.09861	0.00242	3.70073	0.09526	0.27250	0.00597	1598	45	1572	21	1554	30	1
M21-1079-51	0.47	0.06660	0.00145	0.73614	0.01712	0.08026	0.00173	825	45	560	10	498	10	13
M21-1079-52	0.24	0.06881	0.00197	0.75606	0.02225	0.07977	0.00176	893	58	572	13	495	10	16
M21-1079-53	0.18	0.05983	0.00128	0.68496	0.01568	0.08313	0.00179	597	46	530	9	515	11	3
M21-1079-54	0.27	0.07235	0.00158	1.61395	0.03773	0.16198	0.00349	996	44	976	15	968	19	1
M21-1079-55	0.49	0.06148	0.00146	0.69771	0.01751	0.08240	0.00179	656	50	537	10	510	11	5
M21-1079-56	0.30	0.05975	0.00132	0.68385	0.01614	0.08310	0.00179	594	47	529	10	515	11	3
M21-1079-57	0.13	0.07159	0.00153	1.56164	0.03574	0.15839	0.00341	974	43	955	14	948	19	1
M21-1079-58	0.44	0.06028	0.00137	0.68971	0.01668	0.08307	0.00180	614	48	533	10	514	11	4
M21-1079-59	0.50	0.05857	0.00151	0.62172	0.01672	0.07707	0.00168	551	55	491	10	479	10	3
M21-1079-60	1.04	0.06046	0.00169	0.68885	0.01994	0.08273	0.00181	620	59	532	12	512	11	4

(*Continued*)

Table 1. (*Continued*)

M21-1079-61	0.47	0.05743	0.00134	0.64649	0.01599	0.08174	0.00177	508	51	506	10	507	11	0
M21-1079-62	0.27	0.06783	0.00154	0.78863	0.01895	0.08442	0.00183	863	46	590	11	523	11	13
M21-1079-63	0.59	0.05701	0.00134	0.67195	0.01673	0.08558	0.00185	491	52	522	10	529	11	-1
M21-1079-64	0.74	0.06474	0.00143	0.73900	0.01744	0.08288	0.00179	766	46	562	10	513	11	9
M21-1079-65	0.04	0.06812	0.00146	0.77581	0.01778	0.08270	0.00178	872	44	583	10	512	11	14
M21-1079-66	0.26	0.06262	0.00164	0.68591	0.01872	0.07954	0.00173	695	55	530	11	493	10	7
M21-1079-67	0.26	0.05960	0.00141	0.67614	0.01688	0.08238	0.00178	589	50	524	10	510	11	3
M21-1079-68	0.65	0.06779	0.00158	0.75421	0.01858	0.08078	0.00175	862	48	571	11	501	10	14
M21-1079-69	0.44	0.05855	0.00142	0.66528	0.01698	0.08251	0.00179	550	52	518	10	511	11	1
M21-1079-70	0.59	0.05971	0.00252	0.58356	0.02487	0.07096	0.00160	594	89	467	16	442	10	6
M21-1079-71	0.64	0.06084	0.00166	0.68896	0.01956	0.08223	0.00179	634	58	532	12	509	11	4
M21-1079-72	0.43	0.05809	0.00144	0.68165	0.01773	0.08520	0.00185	533	54	528	11	527	11	0
M21-1079-73	0.59	0.06507	0.00362	0.74136	0.04108	0.08273	0.00196	777	113	563	24	512	12	10
M21-1079-74	0.21	0.05663	0.00148	0.65120	0.01771	0.08350	0.00181	476	57	509	11	517	11	-2
M21-1079-75	0.50	0.06260	0.00191	0.73890	0.02313	0.08570	0.00188	695	64	562	14	530	11	6
M21-1079-76	0.27	0.05259	0.00132	0.59709	0.01571	0.08243	0.00179	311	56	475	10	511	11	-7
M21-1079-77	0.03	0.05833	0.00142	0.66749	0.01708	0.08308	0.00180	542	53	519	10	515	11	1
M21-1079-78	0.65	0.06488	0.00157	0.73957	0.01880	0.08276	0.00180	771	50	562	11	513	11	10
M21-1079-79	0.15	0.06034	0.00135	0.68503	0.01629	0.08243	0.00178	616	48	530	10	511	11	4
M21-1079-80	0.46	0.06403	0.00145	0.71541	0.01721	0.08113	0.00175	743	47	548	10	503	10	9
M21-1079-81	0.40	0.05939	0.00142	0.68037	0.01684	0.08324	0.00179	581	51	527	10	515	11	2
M21-1079-82	0.46	0.05708	0.00146	0.65366	0.01719	0.08320	0.00179	494	56	511	11	515	11	-1
M21-1079-83	0.30	0.05732	0.00129	0.64993	0.01526	0.08239	0.00176	503	49	508	9	510	10	0
M21-1079-84	0.14	0.05915	0.00126	0.65299	0.01468	0.08021	0.00171	573	46	510	9	497	10	3
M21-1079-85	0.37	0.05630	0.00133	0.64449	0.01587	0.08318	0.00178	463	52	505	10	515	11	-2
M21-1079-86	1.27	0.06301	0.00343	1.07674	0.05849	0.12416	0.00283	709	112	742	29	755	16	-2
M21-1079-87	0.47	0.05550	0.00467	0.63137	0.05306	0.08266	0.00192	432	178	497	33	512	11	-3
M21-1079-88	0.43	0.06031	0.00163	0.68779	0.01900	0.08286	0.00179	615	57	532	11	513	11	4
M21-1079-89	1.12	0.05551	0.00134	0.63711	0.01593	0.08340	0.00179	433	52	501	10	516	11	-3
M21-1079-90	0.08	0.05880	0.00130	0.66981	0.01551	0.08277	0.00177	560	48	521	9	513	11	2
M21-1079-91	0.12	0.06131	0.00138	0.70632	0.01664	0.08371	0.00179	650	48	543	10	518	11	5
M21-1079-92	0.22	0.06846	0.00166	1.15289	0.02899	0.12236	0.00263	883	49	779	14	744	15	5

(*Continued*)

Table 1. (*Continued*)

Analysis		Corrected ratios						Corrected ages (Ma)						
	Th/U ratios	$^{207}Pb/^{206}Pb$	1σ	$^{207}Pb/^{235}U$	1σ	$^{206}Pb/^{238}U$	1σ	$^{207}Pb/^{206}Pb$	1σ	$^{207}Pb/^{235}U$	1σ	$^{206}Pb/^{238}U$	1σ	Disc %
M21-1079-93	0.53	0.05928	0.00146	0.62389	0.01590	0.07647	0.00164	577	53	492	10	475	10	4
M21-1079-94	0.39	0.06787	0.00181	1.17495	0.03223	0.12579	0.00271	865	54	789	15	764	16	3
M21-1079-95	0.33	0.05442	0.00226	0.59353	0.02458	0.07924	0.00182	389	90	473	16	492	11	-4
M21-1079-96	1.10	0.06185	0.00135	0.68377	0.01562	0.08033	0.00171	669	46	529	9	498	10	6
M21-1079-97	0.38	0.10105	0.00231	4.01751	0.09550	0.28890	0.00622	1643	42	1638	19	1636	31	0
M21-1079-98	0.61	0.05520	0.00127	0.59042	0.01413	0.07772	0.00166	420	50	471	9	483	10	-2
M21-1079-99	0.27	0.05921	0.00150	0.67116	0.01750	0.08237	0.00177	575	54	521	11	510	11	2
M21-1079-100	0.64	0.05634	0.00135	0.58737	0.01460	0.07575	0.00162	465	53	469	9	471	10	0
M21-1079-101	0.80	0.06290	0.00151	0.60612	0.01511	0.07002	0.00150	705	50	481	10	436	9	10
M21-1079-102	0.23	0.09829	0.00213	3.77379	0.08573	0.27898	0.00597	1592	40	1587	18	1586	30	0
M21-1079-103	0.62	0.06325	0.00191	0.74689	0.02307	0.08581	0.00185	717	63	566	13	531	11	7
M21-1079-104	3.15	0.06721	0.00218	1.15383	0.03792	0.12474	0.00274	844	66	779	18	758	16	3
M21-1079-105	0.32	0.05639	0.00124	0.64595	0.01488	0.08323	0.00177	467	48	506	9	515	11	-2
M21-1079-106	0.20	0.06012	0.00137	0.69068	0.01646	0.08348	0.00179	608	49	533	10	517	11	3
M21-1079-107	0.77	0.06161	0.00141	0.70920	0.01692	0.08364	0.00179	661	48	544	10	518	11	5
M21-1079-108	0.38	0.05602	0.00165	0.61406	0.01842	0.07965	0.00172	453	64	486	12	494	10	-2
M21-1079-109	0.48	0.05994	0.00151	0.64173	0.01668	0.07780	0.00167	601	54	503	10	483	10	4
M21-1079-110	0.42	0.06046	0.00188	0.64535	0.02040	0.07756	0.00168	620	66	506	13	482	10	5

Disc.(%) = 100* (207Pb/235U age)/(206Pb/238U age)) -100.

Table 2. U–Pb data for zircons from metasandstone in the Borburgas Formation (Sample M21-2062)

Analysis		Corrected ratios						Corrected ages (Ma)						
	Th/U ratios	$^{207}Pb/^{206}Pb$	1σ	$^{207}Pb/^{235}U$	1σ	$^{206}Pb/^{238}U$	1σ	$^{207}Pb/^{206}Pb$	1σ	$^{207}Pb/^{235}U$	1σ	$^{206}Pb/^{238}U$	1σ	Disc %
M21-2062-01	0.43	0.06110	0.00669	0.99103	0.10741	0.11783	0.00346	643	219	699	55	718	20	-3
M21-2062-02	0.84	0.06368	0.00192	1.03347	0.03243	0.11791	0.00265	731	63	721	16	719	15	0
M21-2062-03	0.61	0.06160	0.00167	1.07028	0.03041	0.12622	0.00284	660	57	739	15	766	16	-4
M21-2062-04	0.55	0.05866	0.00127	0.70397	0.01657	0.08718	0.00193	555	47	541	10	539	11	0
M21-2062-05	1.37	0.09700	0.00217	2.92342	0.07064	0.21895	0.00488	1567	41	1388	18	1276	26	9
M21-2062-06	0.71	0.05797	0.00154	0.67669	0.01897	0.08480	0.00190	528	58	525	11	525	11	0
M21-2062-07	0.03	0.12072	0.00248	5.91586	0.13372	0.35603	0.00787	1967	36	1964	20	1963	37	0
M21-2062-08	0.54	0.05966	0.00152	0.69078	0.01863	0.08412	0.00188	591	54	533	11	521	11	2
M21-2062-09	0.78	0.06491	0.00150	0.75448	0.01867	0.08444	0.00188	772	48	571	11	523	11	9
M21-2062-10	0.63	0.07288	0.00202	1.13113	0.03281	0.11276	0.00254	1011	55	768	16	689	15	12
M21-2062-11	0.51	0.05330	0.00132	0.60617	0.01594	0.08262	0.00184	342	55	481	10	512	11	-6
M21-2062-12	0.01	0.21250	0.00448	16.61717	0.38243	0.56810	0.01264	2925	34	2913	22	2900	52	0
M21-2062-13	0.27	0.06672	0.00156	1.34691	0.03384	0.14665	0.00326	829	48	866	15	882	18	-2
M21-2062-14	0.41	0.07305	0.00189	0.83849	0.02287	0.08339	0.00187	1015	52	618	13	516	11	20
M21-2062-15	0.61	0.05266	0.00141	0.60070	0.01690	0.08287	0.00185	314	60	478	11	513	11	-7
M21-2062-16	0.56	0.07154	0.00205	0.82372	0.02465	0.08365	0.00188	973	57	610	14	518	11	18
M21-2062-17	0.17	0.06745	0.00167	0.77180	0.02025	0.08313	0.00186	852	51	581	12	515	11	13
M21-2062-18	0.60	0.07078	0.00166	1.18039	0.02963	0.12115	0.00270	951	47	792	14	737	16	7
M21-2062-19	0.83	0.05941	0.00138	0.68280	0.01708	0.08350	0.00186	582	50	529	10	517	11	2
M21-2062-20	0.53	0.05356	0.00142	0.60809	0.01696	0.08249	0.00184	352	59	482	11	511	11	-6
M21-2062-21	0.80	0.06261	0.00155	1.01840	0.02679	0.11817	0.00264	695	52	713	13	720	15	-1
M21-2062-22	0.26	0.06109	0.00133	0.69912	0.01657	0.08314	0.00184	642	46	538	10	515	11	5
M21-2062-23	0.27	0.05082	0.00112	0.57839	0.01381	0.08269	0.00183	233	50	463	9	512	11	-10
M21-2062-24	0.27	0.06201	0.00136	0.70653	0.01684	0.08278	0.00183	674	46	543	10	513	11	6
M21-2062-25	0.49	0.06008	0.00172	0.68336	0.02038	0.08264	0.00186	606	61	529	12	512	11	3
M21-2062-26	0.12	0.25759	0.00552	22.60728	0.52721	0.63761	0.01428	3232	33	3210	23	3180	56	1
M21-2062-27	0.09	0.24301	0.00498	20.85641	0.47009	0.62353	0.01379	3140	32	3132	22	3124	55	0
M21-2062-28	0.52	0.05495	0.00149	0.58975	0.01675	0.07797	0.00175	410	59	471	11	484	10	-3
M21-2062-29	0.38	0.08445	0.00227	0.89171	0.02515	0.07671	0.00173	1303	52	647	14	477	10	36
M21-2062-30	0.39	0.05676	0.00132	0.65157	0.01622	0.08340	0.00185	482	51	509	10	516	11	-1

(*Continued*)

Table 2. (*Continued*)

Analysis		Corrected ratios						Corrected ages (Ma)						
	Th/U ratios	$^{207}Pb/^{206}Pb$	1σ	$^{207}Pb/^{235}U$	1σ	$^{206}Pb/^{238}U$	1σ	$^{207}Pb/^{206}Pb$	1σ	$^{207}Pb/^{235}U$	1σ	$^{206}Pb/^{238}U$	1σ	Disc %
M21-2062-31	0.79	0.06765	0.00152	0.77823	0.01885	0.08358	0.00185	858	46	585	11	518	11	13
M21-2062-32	0.12	0.05788	0.00121	0.66552	0.01523	0.08354	0.00185	525	45	518	9	517	11	0
M21-2062-33	0.49	0.07430	0.00160	1.30151	0.03051	0.12726	0.00282	1050	43	846	13	772	16	10
M21-2062-34	0.47	0.06294	0.00149	0.71576	0.01817	0.08261	0.00184	706	50	548	11	512	11	7
M21-2062-35	0.71	0.07065	0.00158	0.80312	0.01938	0.08259	0.00183	947	45	599	11	512	11	17
M21-2062-36	0.41	0.06335	0.00143	1.12709	0.02749	0.12926	0.00287	720	47	766	13	784	16	-2
M21-2062-37	0.53	0.05403	0.00123	0.61195	0.01503	0.08229	0.00183	372	51	485	9	510	11	-5
M21-2062-38	0.58	0.06106	0.00132	0.71238	0.01679	0.08476	0.00188	641	46	546	10	525	11	4
M21-2062-39	0.44	0.07818	0.00214	0.89463	0.02563	0.08314	0.00187	1151	53	649	14	515	11	26
M21-2062-40	0.20	0.05919	0.00125	0.67361	0.01556	0.08268	0.00183	574	45	523	9	512	11	2
M21-2062-41	0.71	0.05715	0.00357	0.64877	0.04023	0.08248	0.00209	497	132	508	25	511	12	-1
M21-2062-42	0.30	0.15333	0.00321	8.88174	0.20334	0.42083	0.00933	2383	35	2326	21	2264	42	3
M21-2062-43	0.69	0.07722	0.00165	0.78343	0.01825	0.07371	0.00163	1127	42	587	10	459	10	28
M21-2062-44	0.45	0.05541	0.00135	0.59287	0.01542	0.07773	0.00173	429	53	473	10	483	10	-2
M21-2062-45	0.43	0.05779	0.00133	0.67278	0.01667	0.08458	0.00188	522	50	522	10	523	11	0
M21-2062-46	0.18	0.11491	0.00262	5.44790	0.13347	0.34444	0.00770	1878	41	1892	21	1908	37	-1
M21-2062-47	0.58	0.07485	0.00212	0.90027	0.02656	0.08738	0.00197	1065	56	652	14	540	12	21
M21-2062-48	0.61	0.06254	0.00136	0.71515	0.01684	0.08308	0.00184	693	46	548	10	515	11	6
M21-2062-49	0.58	0.06225	0.00166	0.79816	0.02238	0.09315	0.00209	683	56	596	13	574	12	4
M21-2062-50	0.44	0.06989	0.00150	0.79042	0.01846	0.08217	0.00182	925	43	591	10	509	11	16
M21-2062-51	0.37	0.05106	0.00114	0.59385	0.01438	0.08450	0.00187	244	51	473	9	523	11	-9
M21-2062-52	0.66	0.07058	0.00160	0.81310	0.01982	0.08369	0.00186	945	46	604	11	518	11	17
M21-2062-53	0.31	0.06722	0.00155	1.26903	0.03138	0.13715	0.00305	845	47	832	14	829	17	0
M21-2062-54	0.59	0.05736	0.00139	0.63488	0.01641	0.08041	0.00179	505	53	499	10	499	11	0
M21-2062-55	0.51	0.05589	0.00122	0.64790	0.01534	0.08422	0.00186	448	47	507	9	521	11	-3
M21-2062-56	0.42	0.06183	0.00134	0.70798	0.01672	0.08319	0.00184	668	46	544	10	515	11	6
M21-2062-57	0.52	0.09499	0.00197	0.98072	0.02231	0.07501	0.00166	1528	39	694	11	466	10	49
M21-2062-58	0.82	0.07397	0.00159	0.74162	0.01738	0.07284	0.00161	1041	43	563	10	453	10	24
M21-2062-59	0.34	0.05913	0.00133	1.00542	0.02439	0.12353	0.00274	572	48	707	12	751	16	-6
M21-2062-60	0.77	0.08478	0.00202	0.95099	0.02413	0.08150	0.00182	1310	46	679	13	505	11	34

(*Continued*)

Table 2. (*Continued*)

M21-2062-61	0.49	0.06051	0.00126	0.73037	0.01670	0.08769	0.00194	622	44	557	10	542	11	3
M21-2062-62	0.62	0.05093	0.00140	0.51458	0.01484	0.07340	0.00163	238	62	422	10	457	10	-8
M21-2062-63	0.08	0.20706	0.00422	15.83274	0.35513	0.55551	0.01226	2883	33	2867	21	2848	51	1
M21-2062-64	0.39	0.07121	0.00149	1.39170	0.03185	0.14198	0.00314	964	42	885	14	856	18	3
M21-2062-65	0.56	0.07055	0.00180	1.22952	0.03316	0.12661	0.00283	944	51	814	15	769	16	6
M21-2062-66	0.45	0.07363	0.00167	1.31491	0.03207	0.12974	0.00288	1031	45	852	14	786	16	8
M21-2062-67	0.49	0.06860	0.00155	0.69491	0.01691	0.07359	0.00163	887	46	536	10	458	10	17
M21-2062-68	0.50	0.05745	0.00125	0.65192	0.01545	0.08244	0.00183	509	48	510	10	511	11	0
M21-2062-69	0.64	0.07654	0.00189	1.34972	0.03547	0.12812	0.00286	1109	49	867	15	777	16	12
M21-2062-70	0.48	0.08804	0.00186	2.68621	0.06203	0.22168	0.00491	1383	40	1325	17	1291	26	3
M21-2062-71	0.47	0.04740	0.00122	0.55647	0.01516	0.08529	0.00190	69	61	449	10	528	11	-15
M21-2062-72	0.25	0.06005	0.00126	0.66044	0.01516	0.07990	0.00177	606	45	515	9	496	11	4
M21-2062-73	0.62	0.19778	0.00406	14.66825	0.33079	0.53880	0.01191	2808	33	2794	21	2778	50	1
M21-2062-74	0.69	0.05313	0.00150	0.54073	0.01600	0.07395	0.00166	334	63	439	11	460	10	-5
M21-2062-75	0.45	0.05925	0.00128	0.67653	0.01592	0.08296	0.00184	576	46	525	10	514	11	2
M21-2062-76	0.84	0.07185	0.00162	0.84175	0.02051	0.08511	0.00189	982	45	620	11	527	11	18
M21-2062-77	0.30	0.06227	0.00139	1.07254	0.02585	0.12513	0.00278	683	47	740	13	760	16	-3
M21-2062-78	0.51	0.05516	0.00121	0.63334	0.01511	0.08342	0.00185	418	48	498	9	517	11	-4
M21-2062-79	0.59	0.17486	0.00360	11.89060	0.26868	0.49403	0.01092	2605	34	2596	21	2588	47	0
M21-2062-80	0.33	0.06377	0.00143	0.78654	0.01902	0.08961	0.00199	734	47	589	11	553	12	7
M21-2062-81	0.43	0.05786	0.00137	0.66889	0.01693	0.08397	0.00185	524	51	520	10	520	11	0
M21-2062-82	0.85	0.09541	0.00256	3.71569	0.10441	0.28287	0.00639	1536	50	1575	22	1606	32	-2
M21-2062-83	0.48	0.06234	0.00160	1.17297	0.03174	0.13666	0.00304	686	54	788	15	826	17	-5
M21-2062-84	0.59	0.07758	0.00182	1.47283	0.03706	0.13789	0.00305	1136	46	919	15	833	17	10
M21-2062-85	1.10	0.05963	0.00139	1.10014	0.02750	0.13399	0.00295	590	50	753	13	811	17	-7
M21-2062-86	0.23	0.22533	0.00477	18.06366	0.41714	0.58226	0.01282	3019	34	2993	22	2958	52	1
M21-2062-87	0.41	0.04828	0.00125	0.54736	0.01498	0.08234	0.00183	113	60	443	10	510	11	-13
M21-2062-88	0.81	0.07375	0.00196	1.37746	0.03857	0.13567	0.00301	1035	53	879	16	820	17	7
M21-2062-89	0.48	0.06050	0.00146	0.74220	0.01911	0.08911	0.00197	621	51	564	11	550	12	2
M21-2062-90	0.50	0.05253	0.00187	0.60260	0.02194	0.08331	0.00189	309	79	479	14	516	11	-7
M21-2062-91	0.55	0.08886	0.00309	1.01324	0.03575	0.08282	0.00193	1401	65	711	18	513	11	39
M21-2062-92	0.93	0.05573	0.00185	1.04060	0.03548	0.13562	0.00307	441	72	724	18	820	17	-12

(*Continued*)

Table 2. (*Continued*)

Analysis		Corrected ratios						Corrected ages (Ma)						
	Th/U ratios	$^{207}Pb/^{206}Pb$	1σ	$^{207}Pb/^{235}U$	1σ	$^{206}Pb/^{238}U$	1σ	$^{207}Pb/^{206}Pb$	1σ	$^{207}Pb/^{235}U$	1σ	$^{206}Pb/^{238}U$	1σ	Disc %
M21-2062-93	0.39	0.06415	0.00155	0.76899	0.01977	0.08707	0.00193	747	50	579	11	538	11	8
M21-2062-94	0.75	0.08880	0.00204	2.80661	0.06914	0.22955	0.00508	1400	43	1357	18	1332	27	2
M21-2062-95	0.50	0.05094	0.00128	0.62495	0.01670	0.08912	0.00197	238	57	493	10	550	12	-10
M21-2062-96	0.44	0.06142	0.00152	0.75420	0.01985	0.08918	0.00198	654	52	571	11	551	12	4
M21-2062-97	0.54	0.08150	0.00280	1.93842	0.06784	0.17276	0.00400	1233	66	1095	23	1027	22	7
M21-2062-98	0.32	0.07226	0.00199	1.70111	0.04912	0.17099	0.00381	993	55	1009	18	1018	21	-1
M21-2062-99	0.28	0.06696	0.00186	0.77228	0.02244	0.08377	0.00187	837	57	581	13	519	11	12
M21-2062-100	0.40	0.08456	0.00194	1.98493	0.04889	0.17049	0.00376	1306	44	1110	17	1015	21	9
M21-2062-101	1.59	0.08165	0.00204	1.91237	0.05049	0.17011	0.00379	1237	48	1085	18	1013	21	7
M21-2062-102	0.75	0.09668	0.00225	3.68079	0.09182	0.27654	0.00613	1561	43	1567	20	1574	31	0
M21-2062-103	0.89	0.05860	0.00245	0.68045	0.02882	0.08435	0.00193	552	89	527	17	522	11	1
M21-2062-104	0.51	0.08412	0.00384	1.04632	0.04811	0.09035	0.00212	1295	86	727	24	558	13	30
M21-2062-105	0.83	0.06129	0.00304	0.67443	0.03353	0.07992	0.00190	650	103	523	20	496	11	6
M21-2062-106	0.61	0.05813	0.00211	0.67918	0.02519	0.08487	0.00193	534	78	526	15	525	11	0
M21-2062-107	1.95	0.18527	0.00451	1.25158	0.03206	0.04907	0.00110	2701	40	824	14	309	7	167
M21-2062-108	0.29	0.08120	0.00189	0.89166	0.02224	0.07976	0.00176	1226	45	647	12	495	11	31
M21-2062-109	0.90	0.05874	0.00175	1.10337	0.03414	0.13642	0.00304	558	64	755	16	824	17	-8
M21-2062-110	0.66	0.06891	0.00203	0.80426	0.02455	0.08477	0.00191	896	60	599	14	525	11	14

Disc.(%) = 100* (207Pb/235U age)/(206Pb/238U age)) -100.

Table 3. U–Pb data for zircons from metasandstone in the Tsengel Formation (Sample M21-1061)

Analysis		Corrected ratios						Corrected ages (Ma)						
	Th/U ratios	$^{207}Pb/^{206}Pb$	1σ	$^{207}Pb/^{235}U$	1σ	$^{206}Pb/^{238}U$	1σ	$^{207}Pb/^{206}Pb$	1σ	$^{207}Pb/^{235}U$	1σ	$^{206}Pb/^{238}U$	1σ	Disc %
M21-1061-01	0.45	0.06878	0.00196	0.78476	0.02419	0.08286	0.00198	892	58	588	14	513	12	15
M21-1061-02	0.96	0.05642	0.00136	1.01469	0.02733	0.13060	0.00308	468	53	711	14	791	18	-10
M21-1061-03	0.43	0.06604	0.00154	1.17439	0.03095	0.12913	0.00305	808	48	789	14	783	17	1
M21-1061-04	0.80	0.05269	0.00158	0.60591	0.01946	0.08351	0.00199	315	67	481	12	517	12	-7
M21-1061-05	0.23	0.05007	0.00120	0.57025	0.01538	0.08270	0.00195	198	55	458	10	512	12	-11
M21-1061-06	0.66	0.06167	0.00147	0.70328	0.01884	0.08281	0.00196	663	50	541	11	513	12	5
M21-1061-07	0.44	0.05693	0.00144	0.66000	0.01850	0.08418	0.00199	488	56	515	11	521	12	-1
M21-1061-08	0.61	0.09919	0.00207	3.82422	0.09267	0.27998	0.00657	1609	38	1598	20	1591	33	0
M21-1061-09	0.70	0.05510	0.00222	0.55963	0.02330	0.07375	0.00181	416	87	451	15	459	11	-2
M21-1061-10	0.73	0.06627	0.00147	1.23112	0.03117	0.13489	0.00317	815	46	815	14	816	18	0
M21-1061-11	0.19	0.06813	0.00153	0.77856	0.01990	0.08298	0.00195	873	46	585	11	514	12	14
M21-1061-12	0.40	0.05717	0.00129	0.64952	0.01669	0.08251	0.00194	497	50	508	10	511	12	-1
M21-1061-13	0.38	0.12143	0.00282	6.01349	0.15739	0.35960	0.00855	1977	41	1978	23	1980	41	0
M21-1061-14	0.30	0.05210	0.00113	0.59442	0.01484	0.08285	0.00195	290	49	474	9	513	12	-8
M21-1061-15	0.80	0.06253	0.00187	0.98201	0.03148	0.11405	0.00272	692	62	695	16	696	16	0
M21-1061-16	0.64	0.05772	0.00131	0.64929	0.01678	0.08169	0.00192	519	49	508	10	506	11	0
M21-1061-17	0.70	0.06477	0.00141	1.14291	0.02863	0.12815	0.00301	767	45	774	14	777	17	0
M21-1061-18	0.71	0.05620	0.00163	0.60079	0.01876	0.07762	0.00185	460	64	478	12	482	11	-1
M21-1061-19	0.71	0.05746	0.00152	0.67056	0.01945	0.08474	0.00201	509	58	521	12	524	12	-1
M21-1061-20	0.35	0.06361	0.00140	0.72469	0.01832	0.08273	0.00195	729	46	553	11	512	12	8
M21-1061-21	1.28	0.06438	0.00159	1.08808	0.02987	0.12272	0.00290	754	51	748	15	746	17	0
M21-1061-22	0.06	0.06949	0.00145	1.42022	0.03442	0.14841	0.00348	913	42	898	14	892	20	1
M21-1061-23	0.08	0.07251	0.00151	1.48117	0.03585	0.14833	0.00348	1000	42	923	15	892	20	3
M21-1061-24	0.86	0.07218	0.00274	0.82745	0.03278	0.08324	0.00200	991	75	612	18	516	12	19
M21-1061-25	0.82	0.06399	0.00159	0.72769	0.02008	0.08258	0.00195	741	52	555	12	512	12	9
M21-1061-26	0.55	0.06140	0.00139	1.10237	0.02835	0.13037	0.00307	653	48	755	14	790	18	-4
M21-1061-27	0.06	0.07865	0.00168	1.76408	0.04355	0.16288	0.00383	1163	42	1032	16	973	21	6
M21-1061-28	1.14	0.06322	0.00169	1.01720	0.02979	0.11685	0.00277	716	56	713	15	712	16	0
M21-1061-29	0.08	0.05524	0.00119	0.63206	0.01574	0.08308	0.00195	422	47	497	10	515	12	-3
M21-1061-30	0.58	0.06647	0.00143	1.23604	0.03061	0.13504	0.00317	821	44	817	14	817	18	0

(*Continued*)

Table 3. (*Continued*)

Analysis		Corrected ratios						Corrected ages (Ma)						
	Th/U ratios	$^{207}Pb/^{206}Pb$	1σ	$^{207}Pb/^{235}U$	1σ	$^{206}Pb/^{238}U$	1σ	$^{207}Pb/^{206}Pb$	1σ	$^{207}Pb/^{235}U$	1σ	$^{206}Pb/^{238}U$	1σ	Disc %
M21-1061-31	0.48	0.06368	0.00177	0.71646	0.02167	0.08169	0.00194	731	58	549	13	506	12	8
M21-1061-32	0.34	0.05155	0.00119	0.58808	0.01534	0.08284	0.00195	266	52	470	10	513	12	-8
M21-1061-33	0.56	0.06676	0.00143	1.20479	0.02985	0.13104	0.00308	830	44	803	14	794	18	1
M21-1061-34	0.69	0.05932	0.00127	0.67571	0.01666	0.08271	0.00194	579	46	524	10	512	12	2
M21-1061-35	0.98	0.06090	0.00146	0.66218	0.01777	0.07896	0.00187	636	51	516	11	490	11	5
M21-1061-36	0.68	0.06204	0.00151	0.67840	0.01849	0.07940	0.00188	676	51	526	11	493	11	7
M21-1061-37	0.67	0.06344	0.00296	0.72256	0.03451	0.08270	0.00205	723	96	552	20	512	12	8
M21-1061-38	0.52	0.06108	0.00137	0.69792	0.01786	0.08297	0.00195	642	48	538	11	514	12	5
M21-1061-39	0.34	0.05771	0.00143	0.64409	0.01778	0.08105	0.00192	519	54	505	11	502	11	0
M21-1061-40	0.47	0.06806	0.00224	1.22974	0.04272	0.13121	0.00317	870	67	814	19	795	18	2
M21-1061-41	0.30	0.05228	0.00112	0.60937	0.01504	0.08465	0.00199	298	48	483	9	524	12	-8
M21-1061-42	0.19	0.07391	0.00156	1.54630	0.03779	0.15192	0.00357	1039	42	949	15	912	20	4
M21-1061-43	0.83	0.06394	0.00135	0.73168	0.01795	0.08310	0.00195	740	44	558	11	515	12	8
M21-1061-44	0.42	0.07284	0.00171	1.51297	0.04007	0.15084	0.00356	1009	47	936	16	906	20	3
M21-1061-45	0.32	0.06133	0.00145	1.11212	0.02965	0.13167	0.00311	651	50	759	14	797	18	-5
M21-1061-46	0.94	0.06235	0.00200	1.11206	0.03780	0.12952	0.00313	686	67	759	18	785	18	-3
M21-1061-47	0.42	0.05026	0.00114	0.58670	0.01515	0.08477	0.00199	207	52	469	10	525	12	-11
M21-1061-48	0.19	0.05774	0.00128	0.66028	0.01674	0.08304	0.00195	520	48	515	10	514	12	0
M21-1061-49	0.42	0.08659	0.00181	2.69037	0.06532	0.22562	0.00529	1351	40	1326	18	1312	28	1
M21-1061-50	0.74	0.06279	0.00140	0.72162	0.01841	0.08346	0.00196	701	47	552	11	517	12	7
M21-1061-51	0.57	0.05041	0.00111	0.57855	0.01464	0.08334	0.00196	214	50	464	9	516	12	-10
M21-1061-52	0.72	0.06022	0.00146	0.68454	0.01857	0.08255	0.00195	611	52	530	11	511	12	4
M21-1061-53	0.59	0.06323	0.00140	0.72611	0.01837	0.08339	0.00196	716	46	554	11	516	12	7
M21-1061-54	0.55	0.06447	0.00151	0.74026	0.01950	0.08338	0.00197	757	49	563	11	516	12	9
M21-1061-55	0.05	0.06101	0.00132	0.99089	0.02473	0.11793	0.00277	640	46	699	13	719	16	-3
M21-1061-56	0.24	0.06642	0.00150	1.26145	0.03237	0.13792	0.00325	820	46	829	15	833	18	-1
M21-1061-57	0.64	0.06993	0.00158	1.44400	0.03703	0.14996	0.00353	926	46	907	15	901	20	1
M21-1061-58	0.78	0.05700	0.00149	0.61000	0.01755	0.07771	0.00184	491	57	484	11	482	11	0
M21-1061-59	0.52	0.06151	0.00150	0.69799	0.01904	0.08240	0.00195	657	52	538	11	511	12	5
M21-1061-60	0.51	0.05769	0.00136	0.65971	0.01751	0.08304	0.00196	518	51	514	11	514	12	0

(*Continued*)

Table 3. (*Continued*)

M21-1061-61	1.75	0.05536	0.00163	0.63981	0.02022	0.08392	0.00201	427	64	502	13	520	12	-3
M21-1061-62	0.45	0.05956	0.00125	0.68761	0.01678	0.08383	0.00197	588	45	531	10	519	12	2
M21-1061-63	0.63	0.06688	0.00147	1.22890	0.03098	0.13342	0.00314	834	45	814	14	807	18	1
M21-1061-64	0.35	0.06472	0.00145	0.73740	0.01886	0.08273	0.00195	765	47	561	11	512	12	9
M21-1061-65	0.66	0.06214	0.00201	0.96356	0.03305	0.11261	0.00271	679	68	685	17	688	16	0
M21-1061-66	0.36	0.05650	0.00121	0.64801	0.01600	0.08328	0.00196	472	47	507	10	516	12	-2
M21-1061-67	0.45	0.04609	0.00113	0.52774	0.01446	0.08315	0.00196	2	58	430	10	515	12	-16
M21-1061-68	0.89	0.05713	0.00127	0.65277	0.01656	0.08296	0.00195	496	49	510	10	514	12	-1
M21-1061-69	0.19	0.06206	0.00145	0.71691	0.01889	0.08389	0.00198	676	49	549	11	519	12	6
M21-1061-70	0.65	0.06044	0.00138	1.01863	0.02635	0.12239	0.00288	619	48	713	13	744	17	-4
M21-1061-71	0.47	0.07194	0.00155	0.82054	0.02039	0.08283	0.00195	984	43	608	11	513	12	19
M21-1061-72	0.55	0.06765	0.00149	0.77837	0.01964	0.08355	0.00197	858	45	585	11	517	12	13
M21-1061-73	0.02	0.13607	0.00282	7.46386	0.18018	0.39833	0.00935	2178	36	2169	22	2161	43	0
M21-1061-74	0.33	0.06552	0.00148	1.36798	0.03508	0.15161	0.00357	791	47	875	15	910	20	-4
M21-1061-75	0.43	0.05905	0.00130	0.68442	0.01723	0.08417	0.00198	569	47	529	10	521	12	2
M21-1061-76	0.60	0.06464	0.00143	0.73899	0.01868	0.08302	0.00195	763	46	562	11	514	12	9
M21-1061-77	0.74	0.06023	0.00132	0.69195	0.01744	0.08342	0.00196	612	47	534	10	517	12	3
M21-1061-78	0.39	0.04940	0.00111	0.56387	0.01442	0.08289	0.00195	167	52	454	9	513	12	-12
M21-1061-79	0.37	0.06755	0.00144	1.24279	0.03065	0.13360	0.00314	855	44	820	14	808	18	1
M21-1061-80	0.86	0.06225	0.00135	0.71399	0.01780	0.08329	0.00196	683	46	547	11	516	12	6
M21-1061-81	1.11	0.06441	0.00163	1.05484	0.02914	0.11888	0.00281	755	53	731	14	724	16	1
M21-1061-82	0.11	0.05444	0.00112	0.61922	0.01465	0.08256	0.00193	389	45	489	9	511	11	-4
M21-1061-83	0.58	0.04648	0.00165	0.53057	0.01952	0.08287	0.00201	22	83	432	13	513	12	-16
M21-1061-84	0.50	0.06322	0.00158	1.17146	0.03208	0.13451	0.00317	716	52	787	15	814	18	-3
M21-1061-85	0.24	0.05859	0.00120	0.68400	0.01610	0.08475	0.00198	552	44	529	10	524	12	1
M21-1061-86	1.48	0.05992	0.00147	1.08220	0.02911	0.13111	0.00309	601	52	745	14	794	18	-6
M21-1061-87	0.62	0.05364	0.00210	0.60924	0.02456	0.08245	0.00202	356	86	483	16	511	12	-5
M21-1061-88	0.34	0.05747	0.00123	0.65876	0.01602	0.08321	0.00195	509	47	514	10	515	12	0
M21-1061-89	0.49	0.04956	0.00117	0.56255	0.01475	0.08239	0.00193	175	54	453	10	510	12	-11
M21-1061-90	0.40	0.06092	0.00138	0.69270	0.01759	0.08253	0.00194	637	48	534	11	511	12	5
M21-1061-91	0.27	0.08614	0.00173	2.74063	0.06355	0.23096	0.00539	1341	38	1340	17	1340	28	0
M21-1061-92	0.34	0.08465	0.00178	2.59052	0.06214	0.22216	0.00520	1307	40	1298	18	1293	27	0

(*Continued*)

Table 3. (*Continued*)

Analysis		Corrected ratios						Corrected ages (Ma)						
	Th/U ratios	$^{207}Pb/^{206}Pb$	1σ	$^{207}Pb/^{235}U$	1σ	$^{206}Pb/^{238}U$	1σ	$^{207}Pb/^{206}Pb$	1σ	$^{207}Pb/^{235}U$	1σ	$^{206}Pb/^{238}U$	1σ	Disc %
M21-1061-93	0.77	0.04836	0.00118	0.55443	0.01490	0.08322	0.00195	117	57	448	10	515	12	-13
M21-1061-94	0.54	0.05555	0.00138	0.65576	0.01792	0.08569	0.00201	434	54	512	11	530	12	-3
M21-1061-95	0.07	0.08491	0.00220	2.66667	0.07490	0.22798	0.00543	1313	50	1319	21	1324	29	0
M21-1061-96	0.59	0.06101	0.00216	0.68252	0.02515	0.08121	0.00194	639	74	528	15	503	12	5
M21-1061-97	0.12	0.05652	0.00129	0.62432	0.01587	0.08019	0.00188	472	50	493	10	497	11	-1
M21-1061-98	0.88	0.12422	0.00252	6.32021	0.14731	0.36934	0.00863	2018	36	2021	20	2026	41	0
M21-1061-99	0.93	0.11271	0.00240	5.07271	0.12268	0.32671	0.00766	1844	38	1832	21	1822	37	1
M21-1061-100	0.89	0.06984	0.00239	1.44109	0.05148	0.14978	0.00363	924	69	906	21	900	20	1
M21-1061-101	0.32	0.06047	0.00125	0.66660	0.01579	0.08002	0.00187	621	44	519	10	496	11	5
M21-1061-102	0.55	0.05283	0.00130	0.56649	0.01533	0.07784	0.00183	322	55	456	10	483	11	-6
M21-1061-103	0.42	0.05872	0.00136	0.67278	0.01727	0.08317	0.00195	557	50	522	10	515	12	1
M21-1061-104	1.41	0.05710	0.00163	0.65415	0.01992	0.08317	0.00198	495	62	511	12	515	12	-1
M21-1061-105	0.36	0.05471	0.00131	0.58304	0.01543	0.07735	0.00182	400	53	466	10	480	11	-3
M21-1061-106	0.56	0.05776	0.00137	0.66619	0.01748	0.08373	0.00196	520	51	518	11	518	12	0
M21-1061-107	0.45	0.05662	0.00195	0.65434	0.02349	0.08389	0.00202	476	75	511	14	519	12	-2
M21-1061-108	0.24	0.05403	0.00125	0.65720	0.01688	0.08829	0.00207	372	51	513	10	545	12	-6
M21-1061-109	0.41	0.06352	0.00136	1.15241	0.02794	0.13171	0.00308	726	45	778	13	798	18	-2
M21-1061-110	1.03	0.05803	0.00139	0.67300	0.01781	0.08419	0.00197	531	52	523	11	521	12	0

Disc.(%) = 100* (207Pb/235U age)/(206Pb/238U age)) -100.

Table 4. U–Pb data for zircons from metasandstone in the Jivertuul Formation (Sample M21-1063/1)

Analysis		Corrected ratios						Corrected ages (Ma)						
	Th/U ratios	$^{207}Pb/^{206}Pb$	1σ	$^{207}Pb/^{235}U$	1σ	$^{206}Pb/^{238}U$	1σ	$^{207}Pb/^{206}Pb$	1σ	$^{207}Pb/^{235}U$	1σ	$^{206}Pb/^{238}U$	1σ	Disc %
M21-1063-01	0.45	0.10746	0.00227	4.68124	0.11433	0.31632	0.00744	1757	38	1764	20	1772	36	0
M21-1063-02	0.52	0.06025	0.00225	0.68735	0.02670	0.08285	0.00201	612	79	531	16	513	12	4
M21-1063-03	0.26	0.06104	0.00134	0.69899	0.01758	0.08316	0.00196	641	47	538	11	515	12	5
M21-1063-05	0.52	0.05078	0.00116	0.55967	0.01448	0.08004	0.00188	231	52	451	9	496	11	-9
M21-1063-06	0.28	0.06729	0.00158	1.17053	0.03085	0.12632	0.00298	847	48	787	14	767	17	3
M21-1063-07	0.40	0.05696	0.00119	0.64781	0.01574	0.08258	0.00194	489	46	507	10	512	12	-1
M21-1063-08	0.28	0.05811	0.00184	0.66238	0.02232	0.08278	0.00199	533	68	516	14	513	12	1
M21-1063-09	0.38	0.05429	0.00118	0.61571	0.01534	0.08235	0.00193	383	48	487	10	510	12	-4
M21-1063-10	0.67	0.05901	0.00142	0.66993	0.01804	0.08244	0.00195	568	52	521	11	511	12	2
M21-1063-11	0.44	0.05402	0.00123	0.61938	0.01602	0.08326	0.00196	372	51	490	10	516	12	-5
M21-1063-12	0.36	0.07692	0.00165	0.89122	0.02202	0.08414	0.00198	1119	42	647	12	521	12	24
M21-1063-13	0.43	0.12557	0.00266	6.36757	0.15574	0.36825	0.00866	2037	37	2028	21	2021	41	0
M21-1063-14	0.14	0.05236	0.00115	0.59603	0.01501	0.08267	0.00194	301	49	475	10	512	12	-7
M21-1063-15	0.63	0.06375	0.00174	1.05309	0.03139	0.11995	0.00285	734	57	730	16	730	16	0
M21-1063-16	0.16	0.06335	0.00139	0.72149	0.01815	0.08271	0.00194	720	46	552	11	512	12	8
M21-1063-17	0.23	0.06444	0.00137	0.73353	0.01798	0.08265	0.00194	756	44	559	11	512	12	9
M21-1063-18	0.57	0.06312	0.00142	0.71696	0.01837	0.08249	0.00194	712	47	549	11	511	12	7
M21-1063-19	0.23	0.06330	0.00146	1.00326	0.02612	0.11509	0.00271	718	48	706	13	702	16	0
M21-1063-20	0.12	0.05359	0.00117	0.63944	0.01601	0.08665	0.00204	354	49	502	10	536	12	-6
M21-1063-21	0.43	0.06442	0.00159	0.73174	0.02009	0.08249	0.00195	755	51	558	12	511	12	9
M21-1063-22	0.57	0.07015	0.00162	0.74041	0.01931	0.07665	0.00181	933	47	563	11	476	11	18
M21-1063-23	0.45	0.05987	0.00129	0.70733	0.01759	0.08580	0.00202	599	46	543	10	531	12	2
M21-1063-24	0.26	0.06872	0.00149	0.81072	0.02022	0.08567	0.00201	890	44	603	11	530	12	14
M21-1063-25	0.30	0.05922	0.00135	0.73247	0.01893	0.08981	0.00212	575	49	558	11	554	13	1
M21-1063-26	0.52	0.07366	0.00171	1.45320	0.03804	0.14325	0.00338	1032	46	911	16	863	19	6
M21-1063-27	0.58	0.05901	0.00174	0.66925	0.02125	0.08236	0.00196	567	63	520	13	510	12	2
M21-1063-28	0.36	0.07490	0.00168	1.43752	0.03670	0.13937	0.00329	1066	44	905	15	841	19	8
M21-1063-29	0.70	0.06848	0.00230	0.76588	0.02696	0.08121	0.00199	883	68	577	16	503	12	15
M21-1063-30	3.87	0.12672	0.00369	6.14659	0.19157	0.35223	0.00864	2053	51	1997	27	1945	41	3
M21-1063-31	0.36	0.13420	0.00312	6.64968	0.17381	0.35983	0.00857	2154	40	2066	23	1981	41	4

(*Continued*)

Table 4. (*Continued*)

Analysis		Corrected ratios						Corrected ages (Ma)						
	Th/U ratios	$^{207}Pb/^{206}Pb$	1σ	$^{207}Pb/^{235}U$	1σ	$^{206}Pb/^{238}U$	1σ	$^{207}Pb/^{206}Pb$	1σ	$^{207}Pb/^{235}U$	1σ	$^{206}Pb/^{238}U$	1σ	Disc %
M21-1063-32	0.42	0.05067	0.00430	0.58909	0.05005	0.08442	0.00225	226	185	470	32	523	13	-10
M21-1063-33	0.32	0.06733	0.00143	0.78063	0.01914	0.08419	0.00198	848	43	586	11	521	12	12
M21-1063-34	0.26	0.07020	0.00152	0.82031	0.02045	0.08486	0.00200	934	44	608	11	525	12	16
M21-1063-35	0.35	0.07154	0.00157	1.33607	0.03365	0.13562	0.00319	973	44	862	15	820	18	5
M21-1063-36	0.48	0.05092	0.00270	0.57817	0.03123	0.08245	0.00201	237	118	463	20	511	12	-9
M21-1063-37	0.36	0.07229	0.00172	1.21590	0.03238	0.12213	0.00289	994	48	808	15	743	17	9
M21-1063-38	0.56	0.07312	0.00170	0.83501	0.02188	0.08293	0.00196	1017	46	616	12	514	12	20
M21-1063-39	0.61	0.06852	0.00152	0.77679	0.01969	0.08233	0.00194	884	45	584	11	510	12	14
M21-1063-41	0.54	0.05943	0.00139	0.67756	0.01790	0.08279	0.00195	583	50	525	11	513	12	2
M21-1063-42	0.40	0.05150	0.00114	0.59795	0.01509	0.08431	0.00198	263	50	476	10	522	12	-9
M21-1063-43	0.12	0.06642	0.00152	0.76930	0.01997	0.08411	0.00198	820	47	579	11	521	12	11
M21-1063-45	0.28	0.07357	0.00156	1.46439	0.03584	0.14455	0.00339	1030	42	916	15	870	19	5
M21-1063-46	0.50	0.06186	0.00136	0.70810	0.01778	0.08313	0.00195	669	46	544	11	515	12	6
M21-1063-47	0.46	0.06218	0.00141	0.71141	0.01831	0.08308	0.00196	680	48	546	11	515	12	6
M21-1063-48	0.50	0.05889	0.00157	0.67010	0.01953	0.08263	0.00196	563	57	521	12	512	12	2
M21-1063-49	0.72	0.06133	0.00239	0.69347	0.02790	0.08211	0.00203	651	81	535	17	509	12	5
M21-1063-50	0.48	0.06686	0.00154	0.74073	0.01929	0.08045	0.00190	833	47	563	11	499	11	13
M21-1063-51	0.28	0.06695	0.00140	0.77675	0.01888	0.08425	0.00198	836	43	584	11	521	12	12
M21-1063-52	0.37	0.05665	0.00129	0.65904	0.01698	0.08448	0.00199	477	50	514	10	523	12	-2
M21-1063-53	0.23	0.06180	0.00131	0.71954	0.01761	0.08454	0.00198	667	45	550	10	523	12	5
M21-1063-54	0.64	0.06909	0.00199	0.66641	0.02069	0.07004	0.00168	901	58	519	13	436	10	19
M21-1063-55	0.33	0.06259	0.00133	0.73023	0.01792	0.08472	0.00199	694	45	557	11	524	12	6
M21-1063-56	0.18	0.05643	0.00119	0.65368	0.01600	0.08412	0.00197	469	47	511	10	521	12	-2
M21-1063-57	0.51	0.05265	0.00173	0.60509	0.02103	0.08346	0.00200	314	73	481	13	517	12	-7
M21-1063-58	0.02	0.13387	0.00275	6.74038	0.16174	0.36563	0.00858	2149	35	2078	21	2009	40	3
M21-1063-59	0.37	0.12744	0.00280	6.36397	0.16003	0.36264	0.00857	2063	38	2027	22	1995	41	2
M21-1063-60	0.29	0.05800	0.00123	0.67681	0.01660	0.08474	0.00199	529	46	525	10	524	12	0
M21-1063-61	0.66	0.06711	0.00151	1.27154	0.03259	0.13758	0.00324	841	46	833	15	831	18	0
M21-1063-62	0.52	0.05105	0.00227	0.55580	0.02548	0.07906	0.00192	243	99	449	17	491	11	-9
M21-1063-63	0.27	0.05571	0.00181	0.60359	0.02078	0.07868	0.00188	440	70	480	13	488	11	-2

(*Continued*)

Table 4. (*Continued*)

M21-1063-64	0.53	0.13527	0.00281	6.89432	0.16666	0.37012	0.00869	2167	36	2098	21	2030	41	3
M21-1063-65	0.69	0.05791	0.00128	0.64085	0.01622	0.08036	0.00189	526	48	503	10	498	11	1
M21-1063-66	0.37	0.05124	0.00112	0.58218	0.01462	0.08251	0.00194	251	50	466	9	511	12	-9
M21-1063-67	0.48	0.07647	0.00170	1.46733	0.03717	0.13933	0.00328	1108	44	917	15	841	19	9
M21-1063-68	0.75	0.07412	0.00246	0.84771	0.02969	0.08306	0.00200	1045	66	623	16	514	12	21
M21-1063-69	0.52	0.18644	0.00386	13.45238	0.32452	0.52396	0.01231	2711	34	2712	23	2716	52	0
M21-1063-70	0.95	0.07565	0.00190	1.34687	0.03742	0.12929	0.00307	1086	50	866	16	784	18	11
M21-1063-71	0.65	0.05539	0.00133	0.62907	0.01695	0.08247	0.00195	428	52	496	11	511	12	-3
M21-1063-72	0.50	0.06124	0.00293	0.69563	0.03381	0.08248	0.00208	648	100	536	20	511	12	5
M21-1063-73	0.64	0.05962	0.00135	0.67695	0.01739	0.08245	0.00194	590	48	525	11	511	12	3
M21-1063-74	0.36	0.12993	0.00273	6.54365	0.15945	0.36571	0.00860	2097	36	2052	21	2009	41	2
M21-1063-75	0.75	0.07080	0.00170	0.92871	0.02494	0.09526	0.00225	952	48	667	13	587	13	14
M21-1063-76	0.50	0.18908	0.00396	13.59493	0.33047	0.52212	0.01229	2734	34	2722	23	2708	52	1
M21-1063-77	0.39	0.05815	0.00129	0.66889	0.01695	0.08353	0.00196	535	48	520	10	517	12	1
M21-1063-78	0.48	0.05222	0.00120	0.59382	0.01546	0.08258	0.00194	295	52	473	10	512	12	-7
M21-1063-79	1.77	0.04813	0.00128	0.53416	0.01561	0.08059	0.00191	106	62	435	10	500	11	-13
M21-1063-81	0.42	0.05476	0.00140	0.63746	0.01807	0.08456	0.00198	403	56	501	11	523	12	-4
M21-1063-82	0.46	0.06996	0.00197	1.35208	0.04146	0.14041	0.00333	927	57	869	18	847	19	3
M21-1063-83	0.56	0.06005	0.00146	0.70153	0.01917	0.08487	0.00199	605	52	540	11	525	12	3
M21-1063-84	0.33	0.05942	0.00138	0.69334	0.01828	0.08477	0.00198	582	50	535	11	525	12	2
M21-1063-85	0.79	0.07097	0.00217	1.40936	0.04620	0.14427	0.00345	957	61	893	19	869	19	3
M21-1063-86	0.33	0.06038	0.00323	0.73284	0.03989	0.08817	0.00217	617	111	558	23	545	13	2
M21-1063-87	0.65	0.05423	0.00191	0.63537	0.02364	0.08512	0.00203	380	77	499	15	527	12	-5
M21-1063-88	1.35	0.06696	0.00191	0.76339	0.02367	0.08282	0.00196	837	58	576	14	513	12	12
M21-1063-89	0.32	0.05957	0.00406	0.69418	0.04734	0.08466	0.00226	588	141	535	28	524	13	2
M21-1063-90	0.74	0.07456	0.00320	1.42475	0.06268	0.13882	0.00345	1056	84	899	26	838	20	7
M21-1063-91	0.43	0.06490	0.00208	0.71585	0.02437	0.08013	0.00192	771	66	548	14	497	11	10
M21-1063-92	1.00	0.07042	0.00166	0.76983	0.02049	0.07942	0.00186	941	47	580	12	493	11	18
M21-1063-93	0.46	0.10888	0.00245	4.76048	0.12247	0.31764	0.00743	1781	40	1778	22	1778	36	0
M21-1063-94	0.54	0.05978	0.00193	0.69354	0.02385	0.08428	0.00200	595	69	535	14	522	12	3
M21-1063-95	0.24	0.06732	0.00149	0.76327	0.01944	0.08236	0.00192	848	45	576	11	510	11	13
M21-1063-96	0.80	0.05781	0.00153	0.67006	0.01953	0.08421	0.00198	522	57	521	12	521	12	0
M21-1063-97	0.55	0.07270	0.00279	1.43353	0.05715	0.14324	0.00348	1006	76	903	24	863	20	5

(*Continued*)

Table 4. (*Continued*)

Analysis	Th/U ratios	Corrected ratios						Corrected ages (Ma)						Disc %
		$^{207}Pb/^{206}Pb$	1σ	$^{207}Pb/^{235}U$	1σ	$^{206}Pb/^{238}U$	1σ	$^{207}Pb/^{206}Pb$	1σ	$^{207}Pb/^{235}U$	1σ	$^{206}Pb/^{238}U$	1σ	
M21-1063-98	0.83	0.06337	0.00178	0.59350	0.01808	0.06803	0.00161	721	58	473	12	424	10	12
M21-1063-99	0.36	0.06048	0.00187	0.70256	0.02324	0.08439	0.00202	621	65	540	14	522	12	3
M21-1063-100	0.37	0.06770	0.00152	0.75348	0.01935	0.08086	0.00189	859	46	570	11	501	11	14
M21-1063-101	0.50	0.07137	0.00308	1.31730	0.05833	0.13409	0.00333	968	85	853	26	811	19	5
M21-1063-102	0.77	0.06802	0.00232	0.79161	0.02857	0.08455	0.00201	869	69	592	16	523	12	13
M21-1063-103	0.99	0.06133	0.00215	0.71454	0.02646	0.08465	0.00201	651	74	547	16	524	12	5
M21-1063-104	0.73	0.06524	0.00231	0.74197	0.02760	0.08262	0.00198	782	73	564	16	512	12	10
M21-1063-105	0.71	0.06616	0.00190	0.77242	0.02400	0.08482	0.00200	811	59	581	14	525	12	11
M21-1063-106	0.29	0.06197	0.00643	0.70541	0.07320	0.08269	0.00221	673	208	542	44	512	13	6
M21-1063-107	0.30	0.06563	0.00152	0.79106	0.02083	0.08757	0.00205	795	48	592	12	541	12	9
M21-1063-108	0.56	0.05850	0.00175	0.66505	0.02147	0.08259	0.00195	549	64	518	13	512	12	1
M21-1063-109	0.62	0.06980	0.00232	1.40496	0.04934	0.14622	0.00352	923	67	891	21	880	20	1
M21-1063-110	0.58	0.05623	0.00160	0.64657	0.01999	0.08354	0.00197	461	62	506	12	517	12	-2

Disc.(%) = 100* (207Pb/235U age)/(206Pb/238U age)) -100.

$^{176}Hf/^{177}Hf$ isotopic ratios of 0.282093–0.282113 and negative $\varepsilon_{Hf}(t)$ values ranging from −7.3 to −3.8. Their T_{DM}^{C} model ages vary from 2.0 to 2.1 Ga. The rest two Mesoproterozoic and Paleoproterozoic zircons have $^{176}Hf/^{177}Hf$ isotopic ratios of 0.280947–0.281848 and $\varepsilon_{Hf}(t)$ values ranging from −30.8 to +1.7 (Fig. 7a). The T_{DM}^{C} model ages range from 2.2 to 4.1 (Table 5).

5.b. Metasandstone from the Borburgas Formation (Sample M21-2062)

A total of one hundred and ten zircon grains were analyzed and twenty-nine analyses for this sample plot below the concordia curve, suggesting a loss of Pb. In the CL images of sample M21-2062, most zircon cores have oscillatory zoning and rounded shapes edge, and 60 – 140 μm, with length-to-width ratios of 1.5:1 to 2.5:1 (Fig. 5b). The zircons display typical oscillatory zoning, and Th/U ratios range from 0.1 to 0.9, indicating a magmatic origin. However, a few zircon grains have Th/U ratios ranging from 0.01 to 0.09 (Table 2), indicating a metamorphic origin.

Analyses on the zircons with oscillatory zoning give concordant U–Pb ages between 456 ± 10 and 3230 ± 33 Ma (Fig. 6d). The ages are mainly clustering at 456–574 Ma, 718–882 Ma, 1012–1335 Ma and 2380–3230 Ma, with the prominent age peak at 517 Ma (n = 44; 54 %), 781 Ma (n = 18; 22 %), and minor peaks at 1299 Ma (n = 7; 9 %), 1921 Ma (n = 4; 5 %) and 2887 Ma (n = 8; 10 %), respectively (Fig. 6e). The youngest coeval zircon grains between 456 ± 10 and 514 ± 11 Ma yield a weighted mean age of 496.6 ± 6.8 Ma (MSWD = 2.53, n = 21) (Fig. 6f).

Fourteen representative zircons were analyzed for Hf isotope compositions. Eight Cambrian and Ordovician zircons have $^{176}Hf/^{177}Hf$ isotopic ratios of 0.282260–0.282379 and their $\varepsilon_{Hf}(t)$ values ranging from −7.6 to −2.9 (except for M21-2062_74 = −54.9). Their T_{DM}^{C} model ages range from 1.7 to –1.9 Ga. Four Neoproterozoic zircons give $^{176}Hf/^{177}Hf$ isotopic ratios varying from 0.282135 to 0.282511. The $\varepsilon_{Hf}(t)$ values and T_{DM}^{C} model ages range from −5.4 to +3.1 and 1.4 to 2.0 Ga. One Mesoproterozoic zircon has a high $^{176}Hf/^{177}Hf$ isotopic ratio of 0.282131 and a positive $\varepsilon_{Hf}(t)$ value of +5.23 (Fig. 7b). T_{DM}^{C} model age is 1.7 Ga (Table 5).

5.c. Metasandstone from the Tsengel Formation (Sample M21-1061)

One hundred and ten zircon grains were dated in the metasandstone *M21-1061*, and ninety-six of them are concordant within error. Zircon grains from a metasandstone sample *M21-1061* are typically short, columnar in shape, rounded and 70–140 μm, with length-to-width ratios of 1.5:1 to 2:1. In CL images, most zircon cores have oscillatory zoning and rounded edges and form two distinct groups: one group consists of euhedral to subhedral grains with concentric oscillatory zoning and a sharp edge (87 %), whereas the other consists of rounded anhedral, homogeneous grains or ones with nebulous zoning (13 %) (Fig. 5c). Most of the zircons with high Th/U ratios range from 0.1 to 1.7, indicating a magmatic origin. The Th/U ratio of a few zircon grains ranges from 0.02 to 0.08, indicating a metamorphic origin (Table 3).

Analyses on the zircons with oscillatory zoning give concordant U–Pb ages ranging from 458 ± 11 to 2175 ± 36 Ma (Fig. 6g). The ages are mainly clustering at 458–529 Ma, 687–972 Ma, 1293–1339 Ma and 1605–2175 Ma, with the prominent age peak at 513 Ma (n = 57, 60 %), 795 Ma (n = 30, 31 %), and minor peaks at 1319 Ma (n = 4, 4 %), and 1995 Ma (n = 5, 5 %), respectively (Fig. 6h). The youngest coeval zircon grains between 458 ± 11 and 506 ± 12 Ma

https://doi.org/10.1017/S0016756824000529 Published online by Cambridge University Press

Table 5. Lu-Hf data for zircons from the metasandstone in the Mongol Altai Group

Sample	$^{176}Yb/^{177}Hf$	2σ	$^{176}Lu/^{177}Hf$	2σ	$^{176}Hf/^{177}Hf$	2σ	εHf(t)	Age	TDM1 (Ma)	TDM2 (Ma)	f(Lu/Hf)
Sample M21-1079/1: Metasandstone from the Maikhant Formation											
M21-1079-21	0.064973	0.001486	0.002023	0.000021	0.282611	0.000024	4.99	515	932	1163	-0.94
M21-1079-26	0.029327	0.000541	0.000967	0.000005	0.282585	0.000022	3.95	494	944	1213	-0.97
M21-1079-50	0.017592	0.001180	0.000640	0.000046	0.280947	0.000024	-30.75	1553	3171	4163	-0.98
M21-1079-57	0.040370	0.002015	0.001202	0.000047	0.282093	0.000018	-3.80	947	1640	2048	-0.96
M21-1079-59	0.019370	0.000830	0.000603	0.000031	0.282456	0.000021	-0.81	478	1113	1503	-0.98
M21-1079-61	0.028342	0.000626	0.001084	0.000011	0.281975	0.000020	-17.42	506	1800	2569	-0.97
M21-1079-63	0.057705	0.001492	0.002037	0.000052	0.282217	0.000020	-8.69	529	1500	2038	-0.94
M21-1079-69	0.024897	0.000738	0.000813	0.000011	0.282585	0.000017	4.39	511	939	1198	-0.98
M21-1079-83	0.048469	0.001850	0.001514	0.000043	0.282671	0.000040	7.16	510	835	1021	-0.95
M21-1079-84	0.025514	0.001533	0.000857	0.000057	0.282442	0.000021	-1.02	497	1141	1530	-0.97
M21-1079-86	0.038035	0.000694	0.001204	0.000007	0.282113	0.000022	-7.28	754	1613	2120	-0.96
M21-1079-95	0.045074	0.001022	0.001346	0.000012	0.282510	0.000025	1.13	491	1059	1390	-0.96
M21-1079-98	0.039865	0.001067	0.001363	0.000017	0.282222	0.000022	-9.27	481	1466	2039	-0.96
M21-1079-100	0.019914	0.000460	0.000727	0.000028	0.282440	0.000022	-1.60	470	1139	1547	-0.98
M21-1079-102	0.025064	0.000252	0.000931	0.000015	0.281848	0.000022	1.65	1586	1967	2196	-0.97
M21-1079-108	0.028293	0.000992	0.001033	0.000041	0.282160	0.000022	-11.11	494	1540	2164	-0.97
Sample M21-2062: Metasandstone from the Borburgas Formation											
M21-2062-40	0.015744	0.000241	0.000664	0.000008	0.282371	0.000015	-3.13	512	1233	1675	-0.98
M21-2062-55	0.049251	0.001809	0.001509	0.000036	0.282356	0.000021	-3.75	521	1282	1721	-0.95
M21-2062-56	0.032451	0.000962	0.001009	0.000040	0.282362	0.000019	-3.49	515	1257	1700	-0.97
M21-2062-64	0.058147	0.003498	0.001661	0.000081	0.282350	0.000026	3.05	856	1296	1547	-0.95
M21-2062-68	0.041979	0.001579	0.001399	0.000036	0.282334	0.000020	-4.72	510	1310	1774	-0.96
M21-2062-70	0.026307	0.000150	0.000871	0.000009	0.282131	0.000018	5.23	1290	1574	1744	-0.97
M21-2062-72	0.032944	0.000737	0.001165	0.000011	0.282260	0.000017	-7.60	495	1406	1945	-0.96
M21-2062-73	0.094725	0.000921	0.002665	0.000047	0.282327	0.000021	42.03	2778	1365	620	-0.92
M21-2062-74	0.119478	0.005436	0.003555	0.000117	0.280964	0.000029	-54.95	460	3403	4843	-0.89
M21-2062-80	0.039836	0.001745	0.001249	0.000042	0.282385	0.000017	-1.97	553	1233	1633	-0.96
M21-2062-88	0.049638	0.001139	0.001767	0.000013	0.282135	0.000020	-5.40	820	1607	2051	-0.95
M21-2062-96	0.107684	0.001316	0.003027	0.000012	0.282511	0.000026	1.81	550	1107	1391	-0.91
M21-2062-103	0.038831	0.001535	0.001267	0.000030	0.282294	0.000022	-5.85	522	1361	1854	-0.96
M21-2062-106	0.035697	0.001500	0.001302	0.000034	0.282376	0.000021	-2.89	525	1247	1670	-0.96

(*Continued*)

Table 5. (*Continued*)

Sample	$^{176}Yb/^{177}Hf$	2σ	$^{176}Lu/^{177}Hf$	2σ	$^{176}Hf/^{177}Hf$	2σ	εHf(t)	Age	TDM1 (Ma)	TDM2 (Ma)	f(Lu/Hf)
Sample M21-1061: Metasandstone from the Tsengel Formation											
M21-1061-09	0.027148	0.000865	0.001016	0.000029	0.282755	0.000027	9.20	459	705	852	-0.97
M21-1061-21	0.059475	0.001844	0.002131	0.000055	0.282116	0.000023	-7.81	746	1650	2146	-0.94
M21-1061-44	0.025385	0.000259	0.000934	0.000016	0.282437	0.000021	7.63	905	1150	1296	-0.97
M21-1061-65	0.046520	0.003437	0.001752	0.000145	0.282335	0.000025	-1.10	515	1321	1680	-0.95
M21-1061-90	0.050457	0.001816	0.001698	0.000065	0.282246	0.000016	-7.93	511	1446	1977	-0.95
M21-1061-92	0.056214	0.001199	0.001766	0.000020	0.282247	0.000018	8.62	1293	1447	1534	-0.95
M21-1061-96	0.018665	0.000732	0.000713	0.000021	0.282341	0.000018	-4.38	503	1276	1748	-0.98
M21-1061-97	0.038138	0.001067	0.001266	0.000020	0.282270	0.000017	-7.23	497	1395	1922	-0.96
M21-1061-99	0.025673	0.001302	0.000850	0.000029	0.281479	0.000020	-6.17	1822	2469	2860	-0.97
M21-1061-102	0.029867	0.000575	0.001026	0.000013	0.282558	0.000021	2.73	483	983	1282	-0.97
M21-1061-103	0.023729	0.000448	0.000813	0.000006	0.282376	0.000024	-2.96	515	1232	1666	-0.98
M21-1061-104	0.087399	0.001293	0.002782	0.000046	0.282298	0.000025	-6.38	515	1413	1882	-0.92
M21-1061-105	0.029525	0.000840	0.000957	0.000013	0.282383	0.000022	-3.50	480	1227	1674	-0.97
M21-1061-106	0.028335	0.000476	0.001078	0.000022	0.282799	0.000020	12.03	518	643	717	-0.97
M21-1061-109	0.052651	0.000302	0.001732	0.000017	0.282328	0.000017	1.00	797	1330	1632	-0.95
Sample M21-1063/1: Metasandstone from the Jivertuul Formation											
M21-1063-1-13	0.023579	0.000475	0.000737	0.000005	0.281496	0.000020	-0.99	2021	2438	2693	-0.98
M21-1063-1-27	0.032305	0.000904	0.001015	0.000017	0.282795	0.000022	11.74	510	647	729	-0.97
M21-1063-1-44	0.033680	0.001632	0.001155	0.000073	0.282450	0.000024	-11.38		1138	1811	-0.97
M21-1063-1-52	0.061763	0.001212	0.001849	0.000037	0.282419	0.000022	-1.60	522	1203	1586	-0.94
M21-1063-1-63	0.021107	0.000383	0.000872	0.000024	0.282805	0.000020	11.66	488	631	717	-0.97
M21-1063-1-65	0.034950	0.000577	0.001304	0.000034	0.282754	0.000022	9.90	498	712	837	-0.96
M21-1063-1-66	0.045061	0.002179	0.001479	0.000059	0.282319	0.000019	-5.26	511	1333	1809	-0.96
M21-1063-1-69	0.033374	0.000297	0.001071	0.000007	0.280996	0.000018	-3.73	2715	3140	3393	-0.97
M21-1063-1-71	0.020525	0.000626	0.000751	0.000012	0.282269	0.000017	-6.81	510	1378	1906	-0.98
M21-1063-1-82	0.010909	0.000258	0.000383	0.000004	0.282214	0.000018	-1.24	847	1440	1811	-0.99
M21-1063-1-84	0.031070	0.001088	0.001000	0.000019	0.282525	0.000020	2.47	524	1028	1330	-0.97
M21-1063-1-85	0.040077	0.000553	0.001407	0.000018	0.281768	0.000020	-17.17	868	2104	2822	-0.96
M21-1063-1-94	0.041382	0.000442	0.001458	0.000015	0.282232	0.000020	-8.12	521	1456	1997	-0.96
M21-1063-1-99	0.029142	0.002005	0.001013	0.000049	0.282355	0.000019	-3.60	522	1267	1712	-0.97
M21-1063-1-108	0.050592	0.001918	0.001735	0.000079	0.282248	0.000021	-7.85	511	1444	1972	-0.95

[a] $T^{C}_{DM} = t + (1/\lambda) * \ln[1 + (((^{176}Hf/^{177}Hf)_{S,t} - (^{176}Hf/^{177}Hf)_{DM,t})/((^{176}Lu/^{177}Hf)_{UC} - (^{176}Lu/^{177}Hf)_{DM})]$, where UC, S and DM are the upper continental crust, the sample and the depleted mantle, respectively. The $^{206}Pb/^{238}U$ ages are used for zircons younger than 1000 Ma, and $^{207}Pb/^{206}Pb$ ages are used for zircons older than 1000 Ma.

Figure 5. Representative cathodoluminescence (CL) images of zircons from the Mongolian Altai Group. Scale bar = 100μm.

https://doi.org/10.1017/S0016756824000529 Published online by Cambridge University Press

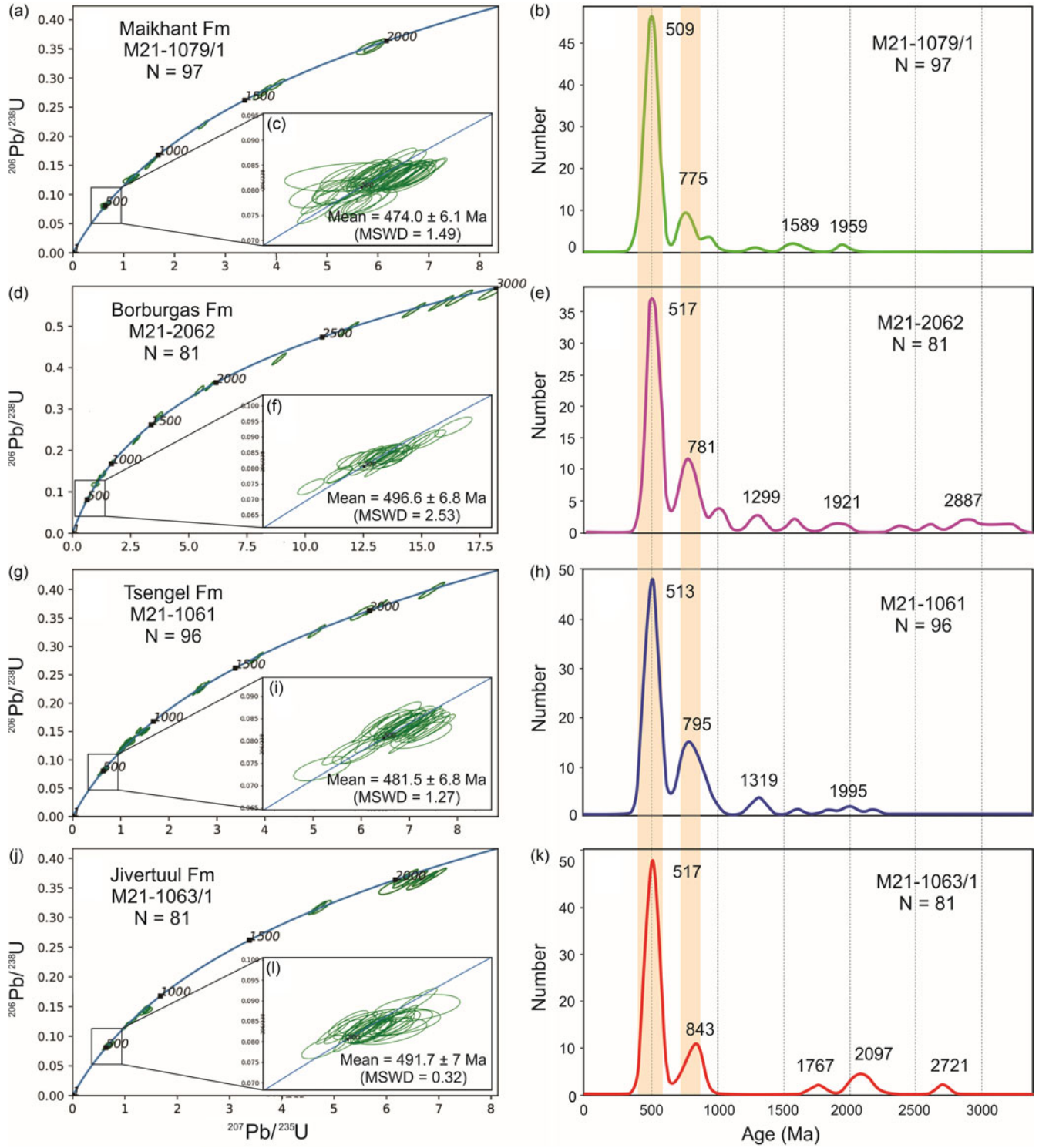

Figure 6. U-Pb concordia and distribution diagrams for detrital zircons of metasandstone from the Mongolian Altai Group. The 206Pb/238U and 207Pb/206Pb ages are used for zircons younger than 1000 Ma and older than 1000 Ma, respectively. Each sample is shown on a separate diagram. See Tables 1–4 for a list of zircon ages.

yield a weighted mean age of 481.5 ± 6.8 Ma (MSWD = 1.27, n = 13) (Fig. 6i).

Fifteen representative zircons from sample *M21-1061* were analyzed for Hf- isotope compositions. Ten Cambrian and Ordovician zircons have high $^{176}Hf/^{177}Hf$ isotopic ratios of 0.282246–0.282799. They have varied εHf(t) values and T_{DM}^{C} model ages ranging from −7.9 to +12.0 and 0.7 to 1.9 Ga, respectively. Three Neoproterozoic zircons give $^{176}Hf/^{177}Hf$ values varying from 0.282116 to 0.282437. The εHf(t) and T_{DM}^{C} model ages range from −7.8 to +7.6 and from 1.3 to 2.1 Ga, respectively. The other two zircons with Mesoproterozoic to Paleoproterozoic ages yield largely varied initial Hf isotopic compositions, with εHf(t) and T_{DM}^{C} model ages varying from −6.2 to +8.6 and 1.5 to 2.8 Ga, respectively (Table 5).

https://doi.org/10.1017/S0016756824000529 Published online by Cambridge University Press

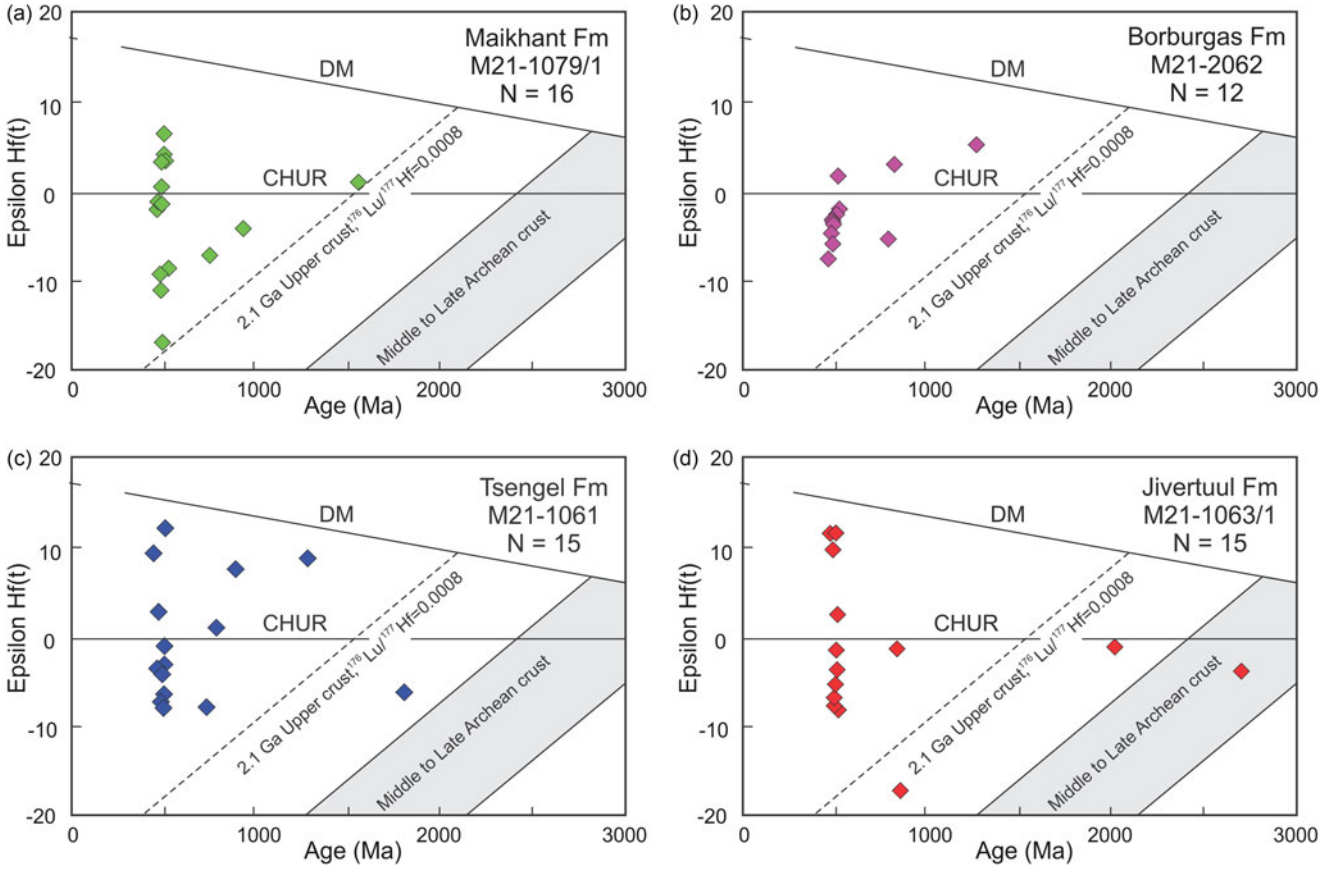

Figure 7. Diagram of ƐHf(t) values versus crystallizing ages for zircons from the Mongolian Altai Group metasandsones. The 206Pb/238U ages are used for zircons younger than 1000 Ma, and 207Pb/206Pb ages are used for zircons older than 1000 Ma.

5.d. Metasandstone from the Jivert-Uul Formation (Sample M21-1063/1)

A total of one hundred and six zircon grains were analyzed and eighty-one of them are concordant within error. In the CL images of sample M21-1063/1, most are subhedral to rounded with oscillatory zoning or nebulous zoning and shapes edge to rounded, and 60–140 μm, with length-to-width ratios of 1:1 to 2:1. A slightly rounded grain in samples 15, 97 and 1 shows a complex internal structure in which a rounded core is surrounded by several low-luminescence layers with variable recrystallized features, and analyses on the core and mantle portions give concordant ages of 730 Ma, 862 Ma and 1.75 Ga, respectively (Fig. 5d). Most of the zircons with high Th/U ratios range from 0.1 to 1.7 (except for M21-1063/1-58 = 0.02), indicating a magmatic origin (Table 4).

Analyses on the zircons with oscillatory zoning give concordant U–Pb ages ranging from 488 ± 12 to 2730 ± 34 Ma (Fig. 6j). The ages are mainly clustering at 488–554 Ma, 702–879 Ma, 1755–1775 Ma, 2035–2165 Ma and 2710–2730 Ma, with the prominent age peak at 517 Ma (n = 54, 66 %), 843 Ma (n = 16, 19 %), and minor peaks at 1767 Ma (n = 2, 3 %), 2097 Ma (n = 7, 9 %), and 2721 Ma (n = 2, 3 %), respectively (Fig. 6k). The youngest coeval zircon grains between 488 ± 12 and 512 ± 12 Ma yield a weighted mean age of 491.7 ± 7 Ma (MSWD = 0.32, n = 25) (Fig. 6l).

Fifteen representative zircons were analyzed for Hf isotope compositions. Ten Cambrian and Ordovician zircons have varied $^{176}Hf/^{177}Hf$ isotopic ratios of 0.282234–0.282805 and $Ɛ_{Hf}(t)$ values ranging from −8.1 to +11.7. Their T_{DM}^{C} model ages varying from 0.7 to 2.0 Ga. Two Neoproterozoic zircons give $^{176}Hf/^{177}Hf$ isotopic ratios varying from 0.281768 to 0.282214. The εHf(t) and T_{DM}^{C} model ages range from −17.2 to −1.2 and from 1.8 to 2.8 Ga, respectively. The other two zircons with Paleoproterozoic and Neoarchean ages all yield low initial Hf isotopic compositions, and εHf(t) values vary from 0.280996 to 0.281496 and from −3.7 to −1.0, respectively (Fig. 7d). Their T_{DM}^{C} model ages range from 2.7 to 3.4 Ga (Table 5).

6. Discussion

6.a. Timing of deposition of metasedimentary rocks

The time of sedimentary deposition must be later than the formation of detrital zircons; the age of the youngest detrital zircon can be used to constrain the maximum age of deposition with the proviso that there was no disturbance in the U-Pb isotopic system (Nelson, 2001; Williams, 2001; Fedo *et al.* 2003). This approach has been successfully applied to sedimentary systems, especially to Precambrian successions where biostratigraphy cannot be used (Bingen *et al.* 2001; Guan *et al.* 2002; Griffin *et al.* 2004; Luo *et al.* 2004; Andersen, 2005; Payne *et al.* 2006; Moecher & Samson, 2006; Xia *et al.* 2006*a*). The Mongolian Altai Group was originally assigned a Middle Cambrian–Lower Ordovician age, but some researchers have suggested a Cambrian or Middle to Upper Cambrian age (Badarch *et al.* 2002; Tovuudorj & Sumya, 2008; Erdenechimeg *et al.* 2018).

https://doi.org/10.1017/S0016756824000529 Published online by Cambridge University Press

Our new study shows that, for the Maikhant and Tsengel Formations, Mongolian Altai Group, the youngest zircon population ages are 474.0 ± 6.1 Ma (sample M21-1079/1) and 481.5 ± 6.8 Ma (sample M21-1061), respectively, indicating their depositional ages must be younger than Lower Ordovician (Figs. 6c, i). While, for the Jivert-Uul and Borburgas Formations in the Mongolian Altai Group, the youngest zircon population ages are 491.7 ± 7 Ma (sample M21-1063/1) and 496.6 ± 6.8 Ma (sample M21-2062), respectively, indicating their depositional ages to be younger than the Guzhangian stage of the Cambrian (Figs. 6f, l). The upper limit of the depositional age of metasedimentary rocks can be constrained by the 450.9 ± 7.8 Ma crystallization age of the Tsagaangol complex intruded into the Mongolian Altai Group. Moreover, metasedimentary rocks of the Mongolian Altai Group are covered by the marine fossil-bearing Tsagaangol Formation, which has a maximum depositional age of 442.4 ± 4 Ma (Narantsetseg *et al.* 2024, unpublished data). All these data indicate that metasedimentary rocks of the Mongolian Altai Group were formed after the Guzhangian stage of the Cambrian and continued to accumulate during the Early-Middle Ordovician in the northern part of the Mongolian Altai.

All samples display a uniform age spectrum that consists of the highest Early Paleozoic age peak at Cambrian, a subdominant peak at Tonian and rare minor peaks with older ages (Fig. 6). Such similar patterns demonstrate that these samples share analogous clastic sources, and the tectonic setting of Mongolian Altai during the Early Paleozoic had not changed remarkably.

6. b. Sedimentary provenance

Based on the U-Pb age data, detrital zircons in the Mongolian Altai flysch sequence can be divided into three populations: an Early Paleozoic, Neoproterozoic and Pre-Neoproterozoic. The detrital zircons from each of the four metasedimentary samples from the Mongolian Altai Group all have a predominant population between 544 and 470 Ma (with main peaks at 517–509 Ma). Additionally, there is a subordinate population with ages between 972 and 687 Ma, showing main peaks at 843–775 Ma, and sparsely distributed between 3.2 and 1.0 Ga (Figs. 6b, e, h and k). These zircon age populations clearly indicate that the provenance of the Mongolian Altai sequence was dominated by rocks from the Neoproterozoic to Early Paleozoic periods. The detrital zircons generally show concentric zoning and high Th/U ratios, which are consistent with an igneous origin. Zircon Hf isotopic compositions indicate that the provenance contained a significant amount of juvenile materials (Fig. 7). Their euhedral shapes suggest that these detrital zircons experienced relatively short sedimentary transport and are probably related to proximal magmatism. On the basis of these lines of evidence, we propose that a Cambrian-Early Ordovician continental arc was the main source for the Mongolian Altai Group sedimentary rocks. More importantly, both the Precambrian blocks and the Lake Zone were intruded by numerous subduction-related granitoids (Kröner *et al.* 2010; Rudnev *et al.* 2012; Soejono *et al.* 2016) of a giant, >1,800 km-long Cambrian Ikh-Mongol arc system (Janoušek *et al.* 2018). These rocks and their eruptive equivalents yielded formation ages between 460 and 520 Ma with a peak around 510 Ma (see summary in Glorie *et al.* 2011; Jiang *et al.* 2011; Rudnev *et al.* 2012; Janoušek *et al.* 2018), exactly matching the predominant zircon population in the studied sedimentary succession.

The Neoproterozoic age populations and the rare older zircons, however, cannot be ignored. These Precambrian grains are well-rounded in shape and have complex internal structures (some of them have a metamorphic rim), suggesting they were likely derived from a more distant source that contained Precambrian materials and possibly that they experienced later metamorphism. Because the Precambrian rocks are absent within the Mongolian Altai sequence and the well-rounded shape of most Precambrian zircons indicates long-distance transportation or recycling, it is unlikely that the Precambrian sediments were derived from nearby sources. The Neoproterozoic zircon population of the Mongolian Altai sequence shows several age peaks at 775, 781, 795 and 843 Ma (Figs. 6b, e, h and k). An analogous Neoproterozoic age distribution was found in the Tuva-Mongol Massif, since new U-Pb dating of detrital zircons from metasediments in this massif revealed Neoproterozoic age peaks at 572, 584, 605 and 876 Ma (Kelty *et al.* 2008). Previous geochronological studies demonstrated that widespread Neoproterozoic magmatism occurred in the Tuva-Mongol Massif and along the southern margin of the Siberian craton (Badarch *et al.* 2002; Tomurtogoo, 2006; Windley *et al.* 2007; Kelty *et al.* 2008). Reasonably, we suggest the areas along the western margin of the Tuva-Mongol microcontinent could be the potential derivation of the subdominant Tonian zircon group. Moreover, older detrital zircon grains (with main peaks at 1.3, 1.9, 2 and 2.8 Ga) were likely derived from coeval felsic magmatism in the Tuva-Mongolian, Zavkhan and Baydrag blocks (Kuzmichev *et al.* 2001; Badarch *et al.* 2002; Kuzmichev *et al.* 2007; Demoux *et al.* 2009; Kuzmichev and Larionov, 2013; Zhang *et al.* 2015e; Bold *et al.*, 2016).

6. c. Implications for the tectonic evolution

The Southern Altai terrane is overlain by Silurian, Devonian and Mississippian volcanic and shallow-marine sedimentary rocks and intruded by Upper Ordovician, Upper Devonian, Carboniferous and Permian granite plutons (Dergunov *et al.* 1980; Gavrilova, 1975).

The terrane contains a high proportion of thrust-imbricated metabasites, suggesting that the rocks were deposited in an arc-proximal setting and later deformed and metamorphosed to greenschist grade (Badarch *et al.*, 2002). The Mongol Altai sedimentary rocks have long been suspected to be of passive continental margin affinity (Zonenshain, 1973); however, Watanabi *et al.* (1994), Mossakovsky, Dergunov (1985) and Byamba, Dejidmaa (1999) argued that the Mongolian Altai sequence was deposited in a forearc/back-arc basin or island arc tectonic settings based on their identification of volcaniclastic sedimentary units. However, some researchers argued that the Mongolian Altai sequence has been formed in a forearc/back-arc basin (Badarch *et al.* 2002; Yakubchuk, 2004; Long *et al.* 2007, 2010; Sun *et al.* 2008; Chen *et al.* 2016; Jiang *et al.* 2011, 2017) or an accretionary prism (Sengör *et al.* 1993; Sengör & Natal'in, 1996; Yuan *et al.* 2007; Sun *et al.* 2008; Long *et al.* 2007, 2008, 2010, Long *et al.*, 2015). Moreover, the Altai-Mongolian terrane used to be interpreted as a remnant of oceanic island arcs that have Late Neoproterozoic–Early Paleozoic age (Buslov *et al.*, 2004 ; Cai *et al.* 2015; Xiao *et al.* 2015, 2018) or a giant accretionary wedge of the Lake Zone of the Ikh-Mongol arc system (Xiao & Kusky, 2009; Soejono *et al.* 2017; Janoušek *et al.* 2018).

Determination of the depositional environment of the studied rocks is difficult due to their metamorphic overprint. However, zircon morphologies and internal structures, together with the distribution of supposed maximum depositional ages, allow for estimating the sedimentary tectonic setting (Cawood *et al.* 2012).

https://doi.org/10.1017/S0016756824000529 Published online by Cambridge University Press

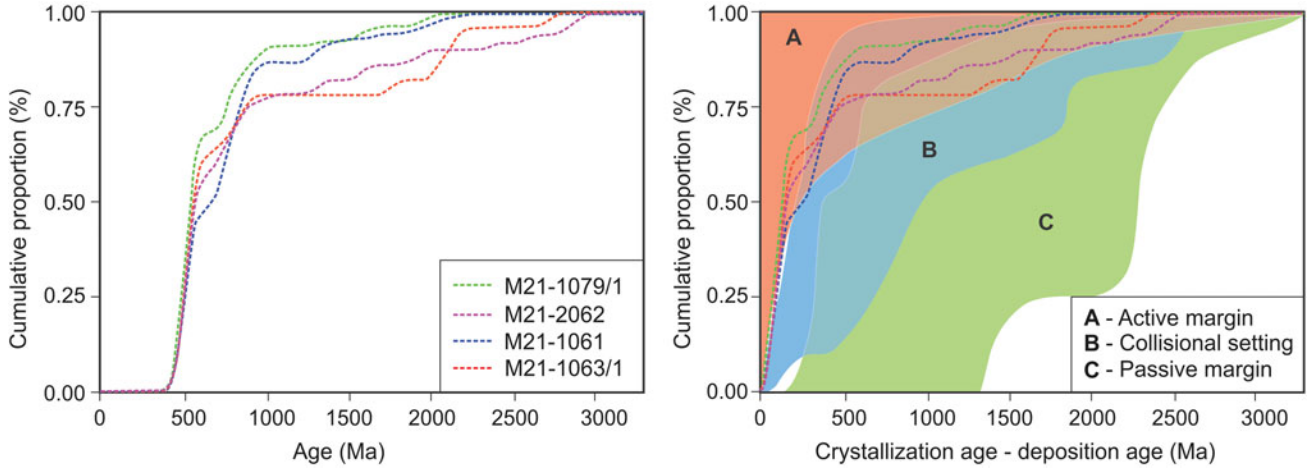

Figure 8. Cumulative distribution curves of detrital zircons from the Early Paleozoic metasedimentary rocks in the Mongolian Altai. The depositional ages of individual units are inferred from the youngest detrital zircon ages. The color fields and reference dashed lines representing different tectonic settings of deposition are after Cawood *et al.,* (2012) and the references therein.

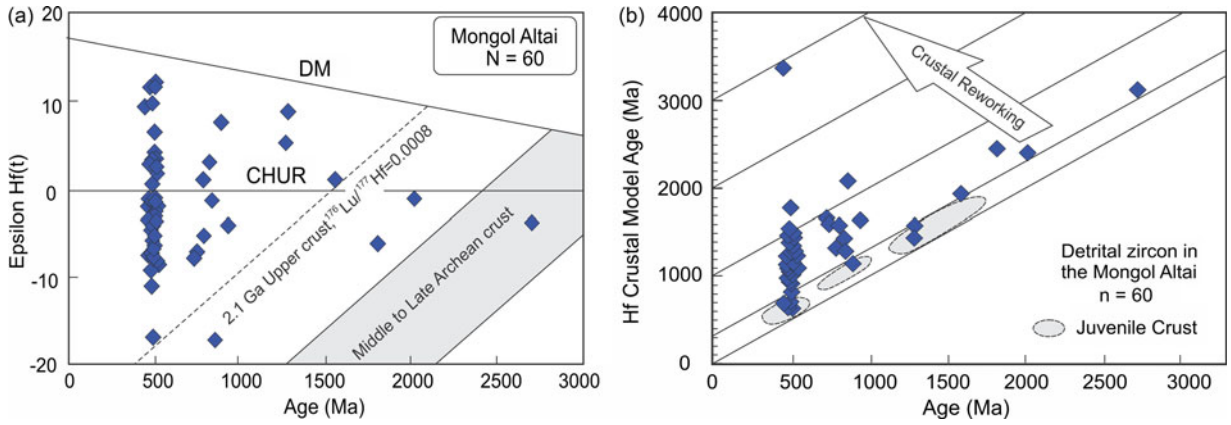

Figure 9. (a) Diagram of ƐHf(t) values versus crystallizing ages for zircons from the Mongolian Altai Group metasandsones. (b) Crystallization age-Hf crustal model age plot of the detrital zircons from the Mongolian Altai Group metasandsones.

All the studied samples are dominated by detrital zircon ages close to their possible age of sedimentation, which indicates an active margin setting in a plot by Cawood *et al.* (2012). This study shows that large amounts of detrital zircons were crystallized in the Early Paleozoic arc magmas derived from mantle or crustal sources. Therefore, our data favour a continental active margin history (Fig. 8).

The similarly supported sources of the Lower Ordovician metasandstones (M21-1079/1 and M21-1061) and the Middle-Upper Cambrian metasandstones (M21-2062 and M21-1063/1) are also supported by their εHf(t) in zircon data. The diagram of εHf(t) versus crystallizing age clearly shows that two important crustal accretion events occurred in the Early Paleozoic and Neoproterozoic in the Mongolian Altai. As shown in the age-εHf(t) diagram (Fig. 9a), the oldest zircon (2.71 Ga, sample M21-1063/1-69) has a Hf crustal model age of ca. 3.14 Ga, which indicates that crustal material of the Altai-Mongolian terrane formed as early as the Mesoarchean. The metasandstone samples show Paleoproterozoic and Neoarchean zircons with mostly negative εHf(t) values, which is a feature typical of the Mongolian Altai zones. However, it is worthwhile to point out that the Mesoproterozoic zircons (1.58–1.29 Ga) mostly have positive εHf(t) values (Fig. 9a) and show that the crustal model ages are <200 Ma larger than their U-Pb ages (Fig. 9b).

Therefore, their positive εHf(t) values represent the addition of juvenile crustal material, which indicates that the Mesoproterozoic is possibly an important period of continental crust growth. The Cambrian to Ordovician zircons reveal both negative and positive εHf(t) values, which is a feature typical for other parts of the Mongolian Altai zones. It is noticeable that ~70% of detrital zircons have negative εHf(t) values, suggesting a synchronous crustal reworking. The Hf isotopic composition of these detrital zircons indicates two crust-forming events that happened in western Mongolia during the Neoproterozoic and Early Paleozoic, respectively. Therefore, it is reasonable to suggest that the subduction process of the Paleo-Asian Ocean in the nearby Ikh-Mongol Arc System caused the Early Paleozoic crustal growth and reworking (Long *et al.* 2019).

Based on recent Lu-Hf isotopic and U-Pb geochronological data for sedimentary rocks, the tectonic evolutionary history of the Mongolian Altai can be reconstructed as follows (Fig. 10). During the Neoproterozoic, a tract of the Paleo-Asian Ocean began to be subducted northward, and a continental arc evolved along the southern margin of the Siberian Craton, resulting in significant continental growth (Fig. 10a), as proposed by Long *et al.* (2010). With the above subduction process continuing, the Tuva-Mongol microcontinent docked with the Siberian Craton, probably during

https://doi.org/10.1017/S0016756824000529 Published online by Cambridge University Press

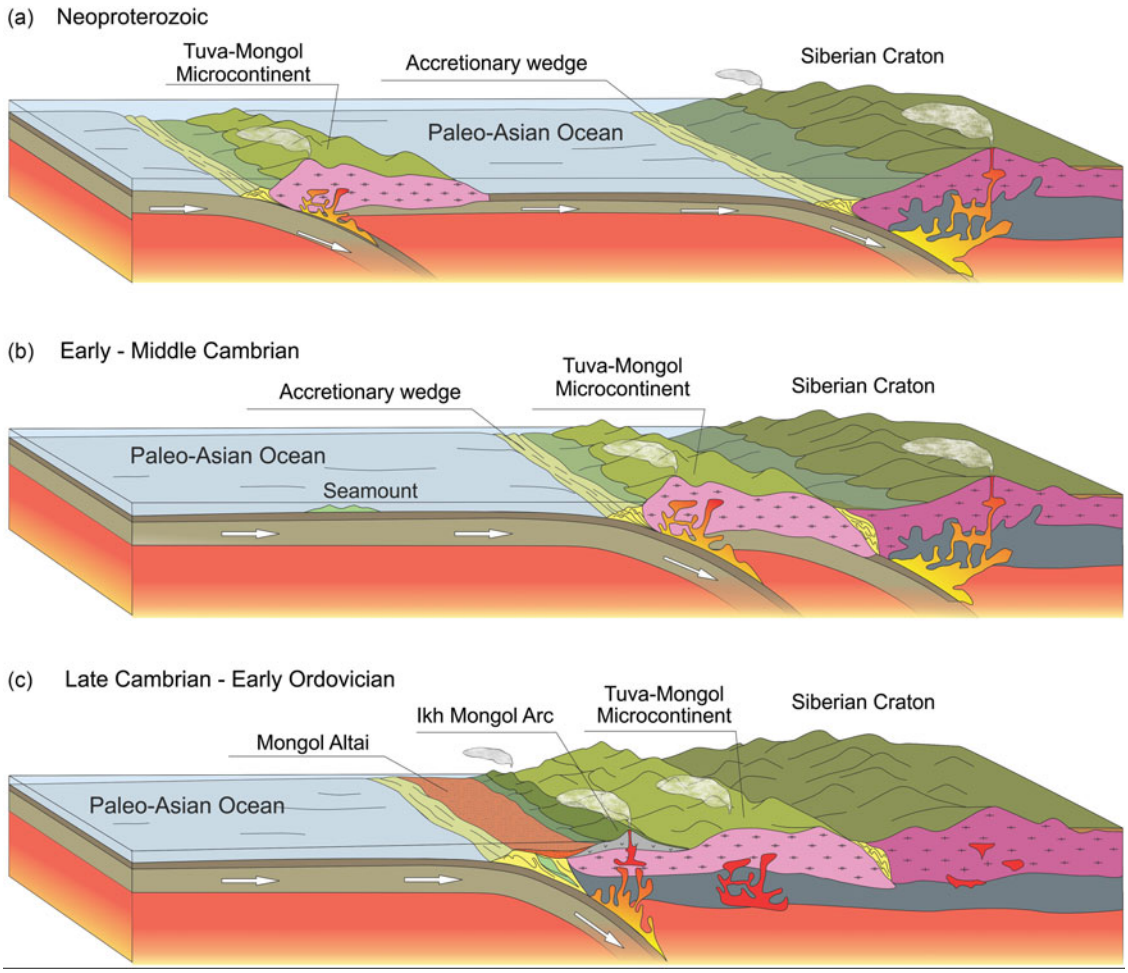

Figure 10. Geodynamic model showing the Neoproterozoic to Ordovician tectonic evolution of the Altai-Mongolian terrane.

the Late Neoproterozoic to Early Paleozoic (Fig. 10b), as suggested by the high-grade metamorphic belt along the southern margin of the Siberian Craton (Khromykh *et al.* 2004; Dobretsov *et al.* 2006; Cai *et al.*, 2014; Li *et al.* 2023a, b). Subsequently, during the Cambrian, a new arc system developed in western Mongolia and started an east-dipping subduction process. Although these tectonic complexes are exotic with respect to the Siberian Craton, they exhibit a close chronological correlation with the arc–back-arc systems surrounding microcontinental blocks in Mongolia (Burianek *et al.* 2017; Khain *et al.* 2003; Kozakov *et al.* 2012; Kröner *et al.* 2011; Lehmann *et al.* 2010; Rudnev *et al.* 2012; Li *et al.* 2023).

Such subduction within the Paleo-Asian Ocean in the Late Cambrian not only significantly reworked the continental sliver but also led to the considerable formation of juvenile crustal material. Large volumes of newly formed arc material and a small number of clastic sediments from the microcontinent and the metamorphic belt were incorporated into the accretionary prism. With continued growth of the accretionary prism, that rollback of the trench caused upwelling of the hot asthenospheric mantle from depth and triggered partial melting of accreted juvenile material to generate widespread granitoids (Long *et al.* 2007, 2010; Jiang *et al.* 2016). In the Cambrian-Ordovician, the Ikh-Mongol arc system was built on the southern of the continental margin, and ocean crust subduction continued (Janoušek *et al.* 2018). In the Late Cambrian, a forearc basin was formed on the accretionary complex, and as a result, the sedimentary sequence of the Mongolian Altai Group began to accumulate (Fig. 10c).

In the Late Ordovician period, the area was intruded by granitoids of the Tsagaangol Complex. After that, it was covered by sedimentary sequences of the Tsagaangol formation, with a sediment accumulation age of 442.4 ± 4.4 Ma (Narantsetseg *et al.* 2024, unpublished data). By the Late Silurian, a regional tectonic uplift took place and was reflected by a regional unconformity recorded by the absence of strata underneath the Early Devonian volcanic rocks.

The Early Paleozoic sedimentary sequences of the Mongolian Altai Group, as a forearc basin, simultaneously received the sediments not only from a newly formed Ikh-Mongol Arc but also from the Neoproterozoic felsic rocks and basement materials of the Tuva-Mongol microcontinent.

6. d. Regional correlation

The Mongolian Altai, located in Western Mongolia, extends to the west and north into China, Kazakhstan and Russia. Regional correlation involves studying the continuity of geological features, rock formations and tectonic structures across these different countries. The understanding of the Mongolian Altai requires collaboration between geologists and researchers from various regions to piece together a comprehensive picture of the orogenic history and its impact on the landscape.

Information from detrital zircons can provide additional palaeogeographic constraints (Cawood *et al.* 2003). High-resolution

https://doi.org/10.1017/S0016756824000529 Published online by Cambridge University Press

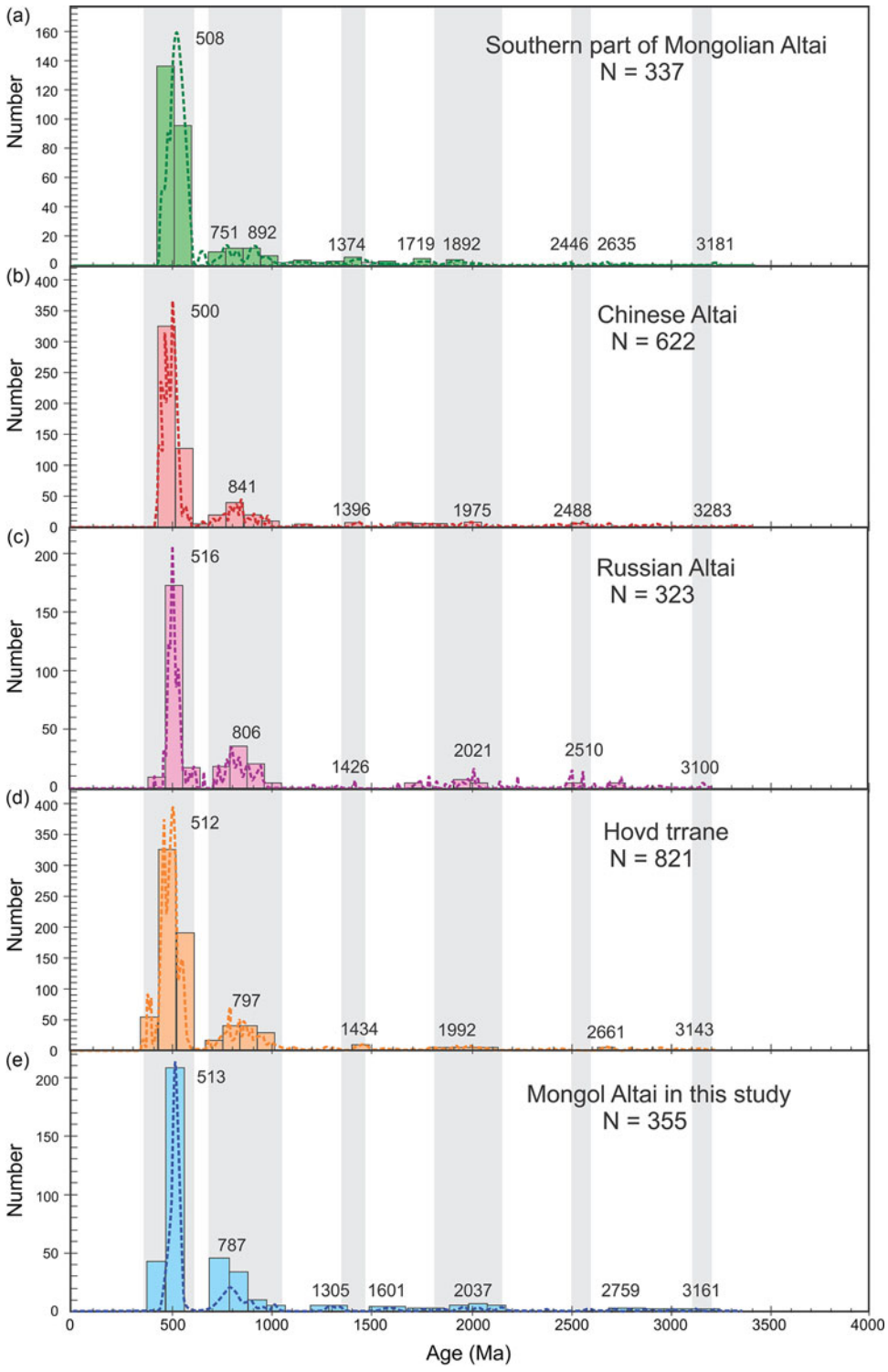

Figure 11. Relative probability plots (concordant data only) for detrital zircons from the (a) southern part of Mongolian Altai (Long *et al.,* 2019), (b) Chinese Altai (Long *et al.,* 2012; Wang *et al.,* 2014; Dong *et al.,* 2018), (c) Russian Altai (Chen *et al.,* 2014; 2016), as well as the adjacent (d) Hovd Zone (Soejono *et al.,* 2018) and (e) Mongolian Altai in this study. (modified from Long *et al.,* 2019).

U-Pb dating of detrital zircons has been conducted for the Mongolian Altai and its adjacent Neoproterozoic-Paleozoic sedimentary rocks in recent years (Buchan *et al.* 2002; Dijkstra *et al.* 2006; Kelty *et al.* 2008; Rojas-Agramonte *et al.* 2011; Salnikova *et al.* 2001; Jiang *et al.* 2011, 2012, 2017; Chen *et al.* 2014, 2016, Long *et al.* 2007, 2008, 2010, 2012, 2019; Yang *et al.* 2011; Soejono *et al.* 2017, 2018; Dong *et al.* 2018; Sukhbaatar *et al.* 2022).

Published data from the Habahe flysch sequence and high-grade metasedimentary rocks from Chinese Altai show similar age spectra and detrital zircons yield a predominant Early Paleozoic age clustering at 460–540 Ma with a minor contribution of Precambrian zircons (Fig. 11). In addition, whole-rock geochemical studies show that the Habahe Group was deposited in an active continental margin or continental arc setting in the Late Ordovician to Silurian, with sources mainly from intermediate-felsic igneous rocks of a nearby magmatic arc (Long *et al.* 2007, 2008, 2010, 2012; Li *et al.*, 2012, 2017, 2019; Chen *et al.* 2014, 2016; Windley *et al.* 2002; Wang *et al.* Wang *et al.*, 2014; Yuan *et al.* 2007;

https://doi.org/10.1017/S0016756824000529 Published online by Cambridge University Press

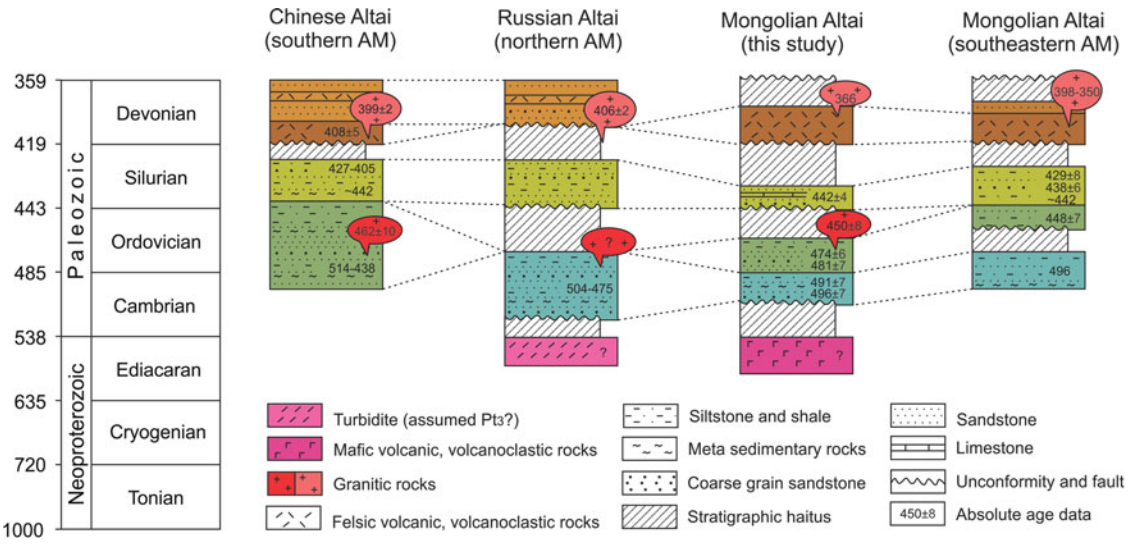

Figure 12. Simplified stratigraphic columns comparing the northern Altai-Mongolian terrane (AM) in the Russian Altai (based on the geological maps of Daukeev *et al.*, 2008; Chen *et al.*, 2014; 2016), the Chinese Altai in northwestern China (after Long *et al.*, 2012; Broussolle *et al.*, 2019), the Mongolian Altai in the southeastern part of Mongolia (after Long *et al.*, 2019), and the Mongolian Altai in western Mongolia (this study).

Sun *et al.* 2008; Cai *et al.* 2011a; Broussolle *et al.* 2019). Precambrian zircon age patterns from these metasedimentary rocks broadly resemble those of the TM block in the northeast and its surrounding arc-related terranes (Jiang *et al.* 2011).

Detrital zircons from the metasedimentary sequences from the Russian Altai also show the most prominent zircon population with Cambrian to Early Ordovician (504–475 Ma) ages, with a subordinate Late Neoproterozoic age (Chen *et al.*, 2015). These rocks were deposited in the early-middle Ordovician, with sediment sources mainly from the Neoproterozoic to early Paleozoic magmatic rocks in the TM and adjacent island arcs (Chen *et al.* 2014, 2015, 2016).

Our new results show that the detrital zircons in the Mongolian Altai flysch sequence have a predominant Cambrian to Early Ordovician population between 544 and 470 Ma (with main peaks at 517–509 Ma) with subordinate Neoproterozoic and Pre-Neoproterozoic age populations. All these zircon age populations clearly indicate that the provenance of the Mongolian Altai sequence was dominated by rocks from the Neoproterozoic to Early Paleozoic periods. Thus, detrital zircon ages from the Russian and Chinese Altai, southern (Jiang *et al.*, 2019) and eastern proximal Hovd terrane (Soejono *et al.* 2017, 2018) parts of Mongolian Altai, closely resemble those observed in the Paleozoic samples from the northern part of Mongolian Altai in our study. For further comparison, detrital zircon age data were compiled from literature on these five regions, as shown in Figure 11.

Thus, our new data, in combination with published detrital zircon data from the Chinese and Russian Altai, as well as from the southern and eastern part of the Mongolian Altai, support point that the Cambrian-Ordovician detrital zircons from metasedimentary rocks from Altai-Mongolian terrane originated from the coeval arc magmatism from the so-called Ikh-Mongol Arc (Janoušek *et al.*, 2018; Li *et al.* 2019; Guy *et al.* 2020; Sukhbaatar *et al.* 2022).

In addition, recent U-Pb dating of detrital zircons from Neoproterozoic to Paleozoic arc-related terranes adjacent to the Tuva-Mongol block revealed that the Tuva-Mongol block significantly contributed the old materials to these sedimentary basins (Kelty *et al.*, 2008; Rojas-Agramonte *et al.*, 2011). Therefore, we suggest that the depositional environment of the Altai-Mongolian terrane, as well as the proximal Hovd terrane, should be alike and uniform in a huge consolidated sedimentary basin that shares analogous provenance during the Early Paleozoic. Apparently, the Mongolian Altai zircons show a quite similar age pattern with those from the Chinese and Russian, i.e., all three of them show similar age peaks at 500–513 Ma, 806 Ma, 1.9 Ga and 2.5 Ga, suggesting a possible identical source of old materials for the three regions. Taken together, all the available data support the idea that the Tuva-Mongol block and the adjacent island arcs were possibly the important sources for the Early Paleozoic metasedimentary rocks in the Mongolian Altai.

According to our study and the results of other researchers, it is plausible that the lithology and depositional age similarities of the sedimentary sequence in Chinese Altai, Russian Altai and Mongolian Altai indicate they were deposited from similar sources in the same basin during the Middle Cambrian to Lower Ordovician periods. This suggests a geological connection between these regions during the Early Paleozoic, possibly indicating a shared depositional environment or geological processes (Fig. 12).

7. Conclusions

On the basis of our U-Pb and Hf isotope data for the detrital zircons from the metasedimentary rocks of the Mongolian Altai, we have the following major conclusions:

1. The metasedimentary rocks of the Mongolian Altai Group were formed after ~497 Ma in the Guzhangian stage of the Cambrian and accumulated during the Early-Middle Ordovician in the northern part of the Altai terrane.
2. The provenance of the metasedimentary rocks in the Mongolian Altai was dominated by Cambrian to Early Ordovician igneous rocks, with subordinate Neoproterozoic and minor Paleoproterozoic and Archean crustal materials. The Tuva-Mongol Massif and adjacent island arc and metamorphic belt may be alternate source regions for the sedimentary sequence in the eastern Mongolian Altai.

https://doi.org/10.1017/S0016756824000529 Published online by Cambridge University Press

3. The Early Paleozoic and Neoproterozoic were important accretionary periods for the Mongolian Altai Group, during which large volumes of juvenile materials were added to the crust. The interpretation of the tectonic setting of the Altai-Mongolian terrane as an active continental margin, possibly acting as a forearc basin, is supported by the geological evidence we have provided.

Supplementary material. The supplementary material for this article can be found at https://doi.org/10.1017/S0016756824000529

Acknowledgements. The authors would like to express their cordial thanks to the staff Institute of Geology of the Mongolian Academy of Sciences and 'Ereen chuluu' LLC, Mongolia for their field assistance and fruitful discussion. Also, we thank Langfang Co., Ltd, China for U-Pb dating. We are very grateful to the associated editor Prof. Peter Clift and the reviewers, whose constructive comments have greatly improved the manuscript.

Financial support. This work was financially supported by the project of 'Integrating of 1:200000 scale State Geology Map of M (N) sheets of Mongolia' implemented by the National Geology Survey of Mongolia.

References

Andersen T (2005) Detrital zircons as tracers of sedimentary provenance: Limiting conditions from statistics and numerical simulation. *Chemical Geology* **216**, 270–94.

Badarch G, Cunningham WD & Windley BF (2002) A new terrane subdivision for Mongolia: implications for the Phanerozoic crustal growth of Central Asia. *Journal of Asian Earth Sciences* **21** (1), 87–110.

Bingen B, Birkeland A, Nordgulen A & Sigmond EMO (2001) Correlation of supracrustal sequences and origin of terranes in the Sveconorwegian orogen of SW Scandinavia: SIMS data on zircon in clastic metasediments. *Precambrian Research* **108**, 293–318.

Blichert-Toft J & Albarede F (1997) The Lu-Hf isotope geochemistry of chondrites and the evolution of the mantle–crust system. *Earth and Planetary Sciences Letters* **148**, 243–58.

Bold U, Crowley JL, Smith EF, Sambuu O & Macdonald FA (2016) Neoproterozoic to early Paleozoic tectonic evolution of the Zavkhan Terrane of Mongolia: implications for continental growth in the Central Asian Orogenic Belt. *Lithosphere* **8**, 729–50.

Briggs SM, Yin A, Manning CE, Chen ZL, Wang XF & Grove M (2007) Late Paleozoic tectonic history of the Ertix fault in the Chinese Altai and its implications for the development of the Central Asian Orogenic system. *Geological Society of America Bulletin* **119**, 944–60.

Broussolle A, Sun M, Schulmann K, Guy A, Aguilar C, Štípská P, JIANG Y & Xiao YYW (2019) Are the Chinese Altai "terranes" the result of juxtaposition of different crustal levels during Late Devonian and Permian orogenesis? *Gondwana Research* **66**, 183–206.

Buchan C, Pfander J, Kröner A, Brewer TS, Tomurtogoo O, Tomurhuu D, Cunningham D & Windley BF (2002) Timing of accretion and collisional deformation in the Central Asian Orogenic Belt: implications of granite geochronology in the Bayankhongor ophiolite zone. *Chemical Geology* **192**, 23–45.

Burianek D, Schulmann K, Hrdliˇ Ckova K, Hanˇ Zl P, Janouˇ Sek V, Gerdes A, & Lexa O (2017) Geochemical and geochronological constraints on distinct Early–Neoproterozoic and Cambrian accretionary events along southern margin of the Baydrag Continent in western Mongolia. *Gondwana Research* **47**, 200–27.

Buslov MM, Fujiwara Y, Iwata K & Semakov NN (2004a) Late Paleozoic–Early Mesozoic Geodynamics of Central Asia. *Gondwana Research* **7**, 791–808.

Buslov MM, Saphonova I, Watanabe T, Obut O, Fujiwara Y, Iwata K, Semakov N, Sugai Y, Smirnova L & Kazansky A (2001) Evolution of the Paleo-Asian Ocean (Altai-Sayan Region, Central Asia) and collision of possible Gondwana-derived terranes with the southern marginal part of the Siberian continent. *Geosciences Journal* **5**, 203–24.

Buslov MM, Watanabe T, Fujiwara Y, Iwata K, Smirnova LV, Safonova, IY, Semakov NN & Kiryanova, AP (2004b) Late Paleozoic faults of the Altai region, Central Asia: tectonic pattern and model of formation. *Journal of Asian Earth Sciences* **23**, 655–71.

Byamba J & Dejidmaa G (1999) Geodynamics of Mongolian Altai. *Mongolian Geoscientist* **3**, 2–25.

Cai KD, Sun M, Jahn BM, Xiao WJ, Yuan C, Long XP, Chen HY & Tumurkhuu D (2015) A synthesis of zircon U–Pb ages and Hf isotopic compositions of granitoids from Southwest Mongolia: implications for crustal nature and tectonic evolution of the Altai Superterrane: *Lithos* **232**, 131–42.

Cai KD, Sun M, Xiao W, Buslov MM, Yuan C, Zhao G & Long X(2014) Zircon U–Pb geochronology and Hf isotopic composition of granitoids in Russian Altai Mountain, Central Asian Orogenic Belt. *American Journal of Science* **314**, 580–612.

Cai KD, Sun M, Yuan C, Long X & Xiao W (2011a) Geological framework and Paleozoic tectonic history of the Chinese Altai, NW China: a review. *Russian Geology and Geophysics* **52**, 1619–33.

Cai KD, Sun M, Yuan C, Zhao G, Xiao W, Long X & Wu F (2011b) Prolonged magmatism, juvenile nature and tectonic evolution of the Chinese Altai, NW China: Evidence from zircon U–Pb and Hf isotopic study of Paleozoic granitoids. *Journal of Asian Earth Sciences* **42**, 949–68.

Cawood PA, Hawkesworth CJ & Dhuime B (2012) Detrital zircon record and tectonic setting: *Geology* **40**, 875–78.

Cawood PA, Nemchin AA, Freeman M & Sircombe K (2003) Linking source and sedimentary basin: detrital zircon record of sediment flux along a modern river system and implications for provenance studies. *Earth and Planetary Science Letters* **210**, 259–68.

Chen M, Sun M, Buslov MM, Cai K, Zhao G, Zheng JP, Rubanova ES & Voytishek EE (2015) Neoproterozoic–middle Paleozoic tectono-magmatic evolution of the Gorny Altai terrane, northwest of the Central Asian Orogenic Belt: constraints from detrital zircon U–Pb and Hf-isotope studies: *Lithos* **233**, 223–36.

Chen, M., Sun, M., Cai, K., Buslov, M. M., Zhao, G. & Rubanova, E. S. (2014) Geochemical study of the Cambrian-Ordovician meta-sedimentary rocks from the northern Altai-Mongolian terrane, northwestern Central Asian Orogenic Belt: Implications on the provenance and tectonic setting. *Journal of Asian Earth Sciences* **96**, 69–83.

Chen M, Sun M, Cai K, Buslov MM, Zhao G, Rubanova ES, Voytishek EE (2014b) *Detrital zircon record of the early Paleozoic meta-sedimentary rocks in Russian Altai: Implications on their provenance and the tectonic nature of the Altai-Mongolian terrane: lithos 3457.*

Chen M, Sun M, Cai K, Buslov MM, Zhao G, Jiang YD, Rubanova ES, Kulikova AV & Voytishek EE (2016) The early Paleozoic tectonic evolution of the Russian Altai: implications from geochemical and detrital zircon U–Pb and Hf isotopic studies of meta-sedimentary complexes in the Charysh-Terekta-Ulagan-Sayan suture zone: *Gondwana Research* **3**, 1–15.

Chu NC, Taylor R, Nesbitt R, Rose MB, Andrew, MJ, German C, Bayon G & Burton K (2002) Hf isotope ratio analysis using multi-collector inductively coupled plasma mass spectrometry: An evaluation of isobaric: *Journal of Analytical Atomic Spectrometry* **17**, 1567–74.

Daukeev SZ, Kim BC, Li T, Petrov OV & Tomurtogoo O. (2008) *Altas Of Geological Maps of Central Asia and Adjacent Areas*. Geological Publishing House.

Demoux A, Kröner A, Badarch G, Jian P, Tomurhuu D, Wingate MTD (2009) Zircon ages from the Baydrag Block and the Bayankhongor Ophiolite Zone: time constraints on Late Neoproterozoic to Cambrian subduction- and accretion-related magmatism in Central Mongolia. *Journal of Geology* **117**, 377–97

Dergunov AB, Kovalenko VI, Ruzhentsev SV & Yarmolyuk VV (2001) *Tectonics, Magmatism, and Metallogeny of Mongolia.* London–New York: Taylor and Francis Group.

Dergunov AB, Luvsandanzan B & Pavlenko VS (1980) Geology of West Mongolia, Nauka, Moscow, 145 p. (in Russian).

Dijkstra AH, Brouwer FM, Cunningham WD, Buchan C, Badarch G & Mason PRD (2006) Late Neoproterozoic proto-arc ocean crust in the Dariv Range, western Mongolia; a type-example of a supra-subduction zone ophiolite. *Journal of the Geological Society London* **163**, 363–73.

Dobretsov NL, Berzin NA & Buslov MM (1995) Opening and tectonic evolution of the Paleo-Asian Ocean. *International Geology Review* **37**, 335–60.

Dobretsov NL, Buslov MM, Zhimulev,FI, Travin AV & Zayachkovsky AA (2006) Vendian–Early Ordovician geodynamic evolution and model for exhumation of ultrahigh- and high-pressure rocks from the Kokchetav subduction–collision zone (northern Kazakhstan). *Russian Geology and Geophysics* **47** (4), 424–40.

Dong ZC, Han YG, Zhao GC, Pan F, Wang K, Huang BT & Chen JL (2018) Zircon U-Pb ages and Hf isotopes of Paleozoic metasedimentary rocks from the Habahe group in the Qinghe area, Chinese Altai and their tectonic implications: *Gondwana Research* **61**, 100–14.

Elhlou S, Belousova E, Griffin WL, Pearson NJ & O'Reilly SY (2006) Trace element and isotopic composition of GJ-red zircon standard by laser ablation. *Geochimica et Cosmochimica Acta* **70** (18), A158. doi: 10.1016/j.gca.2006.06.1383

Erdenechimeg D, Enkhbayar B, Boldbaatar G, Damdinjav B & Taivanbaatar TS (2018) Geological map of Mongolia. scale 1:500,000.

Fedo CM, Sircombe KN & Rainbird RH (2003) Detrital zircon analysis of the sedimentary record. *Reviews in Mineralogy and Geochemistry* **53**, 277–303.

Gavrilova SP (1975) Granitoid formations of Western Mongolia. In Granitoid and Alkaline Formations in the Structures of Western and Northern Mongolia. *Transactions* **14**, 50–143.

Glorie S, De Grave J, Buslov MM, Zhimulev FI, Izmer A, Vandoorne W, Ryabinin A, Van Den Haute P, Vanhaecke F & Elburg MA (2011) Formation and Palaeozoic evolution of the Gorny-Altai–Altai-Mongolia suture zone (South Siberia): Zircon U/Pb constraints on the igneous record. *Gondwana Research* **20**, 465–84.

Griffin WL, Belousova EA, Shee SR, Pearson NJ & O'Reilly SY (2004) Archaean crustal evolution in the northern Yilgarn Craton: U-Pb and Hf isotope evidence from detrital zircons. *Precambrian Research* **131**, 231–82.

Guan H, Sun M, Wilde SA, Zhou XH & Zhai MG (2002) SHRIMP U-Pb zircon geochronology of the fuping complex: implications for formation and assembly of the North China craton. *Precambrian Research* **113**, 1–18.

Guy A, Schulmann K, Soejono I, & Xiao W (2020) Revision of the Chinese Altai-East Junggar terrane accretion model based on geophysical and geological constraints. *Tectonics* **39**, 1–24

Hanchar JM & Hoskin PWO (2003) Zircon. *Reviews in Mineralogy and Geochemistry* **53**, 500.

Hou ZQ, Pan XF, Yang ZM & Qu XM (2007) Porphyry Cu–(Mo–Au) deposits no related to oceanic-slab subduction: examples from Chinese porphyry deposits in continental settings. *Geoscience* **21**, 332–51.

Hu A, Jahn B, Zhang G, Chen Y & Zhang Q (2000) Crustal evolution and Phanerozoic crustal growth in northern Xinjiang: Nd isotopic evidence. Part I. Isotopic characterization of basement rocks. *Tectonophysics* **328**, 15–51.

Janoušek V, Jiang YD, Buriánek D, Schulmann K, Hanžl P, Soejono I, Kröner A, Altanbaatar B, Erban V, Lexa O, Ganchuluun T & Košler J (2018) Cambrian–Ordovician magmatism of the Ikh-Mongol arc system exemplified by the Khantaishir Magmatic Complex (Lake Zone, south-central Mongolia). *Gondwana Research* **54**, 122–49.

Jiang YD, Schulmann K, Sun M, Weinberg RF, Štípská P & Li PF (2019) Structural and geochronological constraints on Devonian suprasubduction tectonic switching and Permian collisional dynamics in the Chinese Altai, central Asia. *Tectonics*, **38**(1), 253–80.

Jiang YD, Schulmann K, Kröner A, Sun M, Lexa O, Janoušek V, Buriánek D, Yuan C & Hanžl P (2017) Neoproterozoic–early Paleozoic peri-Pacific accretionary evolution of the Mongolian collage system: Insights from geochemical and U-Pb zircon data from the Ordovician sedimentary wedge in the Mongolian Altai. *Tectonics* **36**, 2305–31.

Jiang YD, Schulmann K, Sun M, Štípská P, Guy A, Janoušek V, Lexa O, Yuan C, (2016) Anatexis of accretionary wedge, Pacific-type magmatism, and formation of vertically stratified continental crust in the Altai Orogenic Belt. *Tectonics* **35**, 3095–118.

Jiang YD, Sun M, Kröner A, Tumurkhuu D, Long X, Zhao G, Yuan C & Xiao W (2012) The high-grade Tseel Terrane in SW Mongolia: An Early Paleozoic arc system or a Precambrian sliver? *Lithos* **142–143**, 95–115.

Jiang YD, Sun M, Zhao G, Yuan C, Xiao W, Xia X, Long X & Wu F (2011) Precambrian detrital zircons in the Early Paleozoic Chinese Altai: their provenance and implications for the crustal growth of central Asia. *Precambrian Research* **189**, 140–54.

Kelty TK, Yin A, Dash B, Gehrels, GE & Ribeiro AE (2008) Detrital-zircon geochronology of Paleozoic sedimentary rocks in the Hangay-Hentey basin, north-central Mongolia: implications for the tectonic evolution of the Mongol Okhotsk Ocean in central Asia. *Tectonophysics* **451**, 97–122.

Khain EV, Bibikova EV, Salnikova EB, Kröner A, Gibsher AS, Didenko AN, Degtyarev KE, & Fedotova AA (2003) The Palaeo-Asian ocean in the Neoproterozoic and early Palaeozoic: New geochronologic data and palaeotectonic reconstructions. *Precambrian Research* **122**(1–4), 329–58.

Khromykh EV, Sergeev SA, Matukov DI, Vladimirov AG, Mekhonoshin AS, Fedorovsky VS, Volkova NI, Rudnev SN, Khlestov VV & Yudin DS (2004) U–Pb age (SHRIMP-II) of hypersthene plagiogranites of the Chernorudskaya granulitic zone (Ol'khon region,West Transbaikalia). Geodynamic evolution of the lithosphere of the Central Asian mobile belt (fromocean to continent), Inst. *Geograph. Publ*, **1**, 141–45.

Koschek G (1993) Origin and significance of the SEM cathodoluminescence from zircon. *Journal of Microscopy* **171**, 223–32.

Kozakov IK, Sal'nikova EB, Yarmolyuk VV, Kozlovsky AM, Kovach VP, Azimov, PY, Anisimova IV, Lebedev VI, Enjin G, Erdenejargal C, Plotkina YV, Fedoseenko, AM, & Yakovleva SZ (2012) Convergent boundaries and related igneous and metamorphic complexes in caledonides of Central Asia. *Geotectonics* **46**(1), 16–36.

Kröner A, Demoux A, Zack T, Rojas-Agramonte Y, Jian P, Tomurhuu D, & Barth M (2011) Zircon ages for a felsic volcanic rock and arc-related early Palaeozoic sediments on the margin of the Baydrag microcontinent, central Asian orogenic belt, Mongolia. *Journal of Asian Earth Sciences* **42**(5), 1008–17.

Kröner A, Lehmann J, Schulmann K, Demoux A, Lexa O, Tomurhuu D, Štípská P, Liu D & Wingate MTD (2010) Lithostratigraphic and geochronological constraints on the evolution of the Central Asian Orogenic Belt in SW Mongolia: Early Paleozoic rifting followed by late Paleozoic accretion. *American Journal of Science* **310**, 523–74.

Kuzmichev AB, Bibikova EV, Zhuravlev DZ (2001) Neoproterozoic (~800 Ma) orogeny in the Tuva-Mongolia Massif (Siberia): island arc–continent collision at the northeast Rodinia margin. *Precambrian Research* **110**, 109–26.

Kuzmichev AB, Larionov AN (2013) Neoproterozoic island arcs in East Sayan: duration of magmatism (from U–Pb zircon dating of volcanic clastics). *Russian Geology and Geophysics* **54**, 34–43.

Kuzmichev AB, Sklyarov E, Postnikov A, Bibikova E (2007) The Oka Belt (Southern Siberia and Northern Mongolia): a Neoproterozoic analog of the Japanese Shimanto Belt? *Island Arc* **16**, 224–42.

Lehmann J, Schulmann K, Lexa O, Corsini M, Kroner A, Stipska P, Tomurhuu D, & Otgonbator D (2010) Structural constraints on the evolution of the central Asian Orogenic Belt in SW Mongolia. *American Journal of Science* **310**(7), 575–628.

Li HJ, He GQ, Wu TR & Wu B (2006) Confirmation of Altai-Mongolia microcontinent and its implications. *Acta Petrological Sinica* **22**, 1369–79 (in Chinese with English abstract).

Li HJ, Tang GQ Gond B Yang YH Hou KJ Hu ZCH Li QL & Liu Y (2013) Qinghu zircon: A working reference for microbeam analysis of U-Pb age and Hf and O isotopes. *Chinese Science Bulletin* **58**, 4647–54.

Li, P, Sun, M, Rosenbaum, G, Jourdan, F, Li, S & Cai, K (2017) Late Paleozoic closure of the Ob-Zaisan Ocean along the Irtysh shear zone (NW China): implications for arc amalgamation and oroclinal bending in the Central Asian orogenic belt. *Geol. Soc. Am. Bull.* **129**, 547–69.

Li P, Sun M, Shu CH, Yuan CH, Jiang Y, Zhang L, Cai K (2019) Evolution of the Central Asian Orogenic Belt along the Siberian margin from Neoproterozoic-Early Paleozoic accretion to Devonian trench retreat and a comparison with Phanerozoic eastern Australia. *Earth-Science Reviews* **198**, 102951.

Li XH, Li ZX, He B, Li WX, Li QL, Gao YY & Wang XC (2012) The Early Permian active continental margin and crustal growth of the Cathaysia Block: In situ U–Pb, Lu–Hf and O isotope analyses of detrital zircons. *Chemical Geology*, **328**, 195–207.

Li Z, Jiang Y, Collett S, Štípská P, Schulmann K, Wang S, Sukhorukov V, (2023) Metamorphic and chronological constraints on the early Paleozoic tectono-thermal evolution of the Olkhon Terrane, southern Siberia. *Journal of Metamorphic Geology* **41**, 525–56.

Li ZY, Jiang YD, Collett S, Štípská P, Schulmann K, Wang S, Sukhorukov V, Bai XJ, Zhang WF, (2023) Peri-Siberian Ordovician to Devonian Tectonic switching in the Olkhon Terrane (Southern Siberia): Structural and Geochronological Constraints. *Tectonics* **42**, e2023TC007826

Long XP, Luo J, Sun M, Wang X, Wang Y, Yuan CH, & Jiang Y (2019) Detrital zircon U-Pb ages and whole-rock geochemistry of early Paleozoic metasedimentary rocks in the Mongolian Altai: Insights into the tectonic affinity of the whole Altai-Mongolian terrane. *GSA Bulletin* **132**(3-4), 477–94. doi: 10.1130/B35257.1.

Long XP, Sun M, Yuan C, Xiao W & Cai K, (2008) Early Paleozoic sedimentary record of the Chinese Altai: implications for its tectonic evolution. *Sedimentary Geology* **208**, 88–100.

Long XP, Sun M, Yuan C, Xiao WJ, Lin SF, Wu FY, Xia XP & Cai KD (2007) U–Pb and Hf isotopic study of zircons from metasedimentary rocks in the Chinese Altai: implications for Early Paleozoic tectonic evolution. *Tectonics* **26**, TC5015. doi: 10.1029/2007TC002128.

Long XP, Wilde SA, Yuan C, Hu AQ & Sun M (2015) Provenance and depositional age of Paleoproterozoic metasedimentary rocks in the Kuluketage Block, northern Tarim Craton: Implications for tectonic setting and crustal growth: *Precambrian Research* **260**, 76–90.

Long XP, Yuan C, Sun M, Safonova I, Xiao W & Wang Y (2012) Geochemistry and U–Pb detrital zircon dating of Paleozoic graywackes in East Junggar, NW China: insights into subduction–accretion processes in the southern Central Asian Orogenic Belt. *Gondwana Research* **21**(2-3), 637–53.

Long XP, Yuan C, Sun M, Xiao W, Zhao G, Wang Y, Cai K, Xia X & Xie L (2010) Detrital zircon ages and Hf isotopes of the early Paleozoic flysch sequence in the Chinese Altai, NW China: New constrains on depositional age, provenance and tectonic evolution. *Tectonophysics* **480**, 213–31.

Ludwig KR (2003) ISOPLOT 3: A geochronological Toolkit for Microsoft excel. *Berkeley Geochronology Centre Special Publication* **4**, 74.

Luo Y, Sun M, Zhao GC, Li SZ, Xu P, Ye K & Xia XP (2004) LA-ICP-MS U – Pb zircon ages of the Liaohe Group in the Eastern Block of the North China Craton: Constraints on the evolution of the Jiao-Liao-Ji Belt. *Precambrian Research* **134**, 349–71.

Moecher DP & Samson SD (2006) Differential zircon fertility of source terranes and natural bias in the detrital zircon record: Implications for sedimentary provenance analysis. *Earth and Planetary Science Letters* **247**, 252–66.

Mossakovsky A, Ruzhentsev S, Samygin S & Kheraskova T (1994) Central Asian fold belt: Geodynamic evolution and formation history. *Geotectonics* **27**, 445–74.

Mossakovsky AA & Dergunov AB (1985) The Caledonides of Kazakhstan, Siberia, and Mongolia: a review of structure, development history, and palaeotectonic environments. In: *The Caledonide Orogen-Scandinavia and Related Areas* (eds D.G. Gee, B.A. Sturt, pp. 1201–15. London: Wiley.

Narantsetseg TS, Oyunchimeg T, Udaanjargal KH & Batzorig G, (2024) Geological map of Mongolia (scale 1:200,000): Ulaanbaatar, "M-200" project of Ereen Chuluu LLC. Unpublished.

Nelson DR (2001) An assessment of the determination of depositional ages for Precambrian clastic sedimentary rocks by U–Pb dating of detrital zircon. *Sedimentary Geology* **141–142**, 37–60.

Payne JL, Barovich KM & Hand M (2006) Provenance of metasedimentary rocks in the northern Gawler Craton, Australia: implications for palaeoproterozoic reconstructions, *Precambrian Research* **148**, 275–91.

Pearce CL (1997) The determinants of changemanagement team (CMT) effectiveness: A longitudinal investigation. Unpublished doctoral dissertation, University of Maryland, College Park.

Rojas-Agramonte Y, Kröner A, Demoux A, Xia X, Wang W, Donskaya T, Liu D & Sun M (2011) Detrital and xenocrystic zircon ages from Neoproterozoic to Paleozoic arc terranes of Mongolia: Signi cance for the origin of crustal fragments in the Central Asian Orogenic Belt. *Gondwana Research* **19**, 751–63.

Rudnev SN, Izokh AE, Borisenko AS, Shelepaev RA, Orihashi Y, Lobanov KV & Vishnevsky AV (2012) Early Paleozoic magmatism in the Bumbat–Hairhan area of the Lake Zone in western Mongolia (geological, petrochemical, and geochronological data). *Russian Geologyand Geophysics, Geologiya i Geofizika* **53** (5), 425–41 (557–78).

Salnikova EB, Kozakov IK, Kotov AB, Kroner A, Todt W, Bibikova EV, Nutman A, Yakovleva, SZ & Kovach VP (2001) Age of Palaeozoic granites and metamorphism in the Tuvino-Mongolian Massif of the Central Asian Mobile Belt: loss of a Precambrian microcontinent. *Precambrian Research* **110**, 143–64.

Scherer E, Munker C & Mezger K (2001) Calibration of the Lutetium–Hafnium clock. *Science* **293**, 683–87.

Sengör AMC, Natal'in BA & Burtman VS (1993) Evolution of the Altaid tectonic collage and Palaeozoic crustal growth in Eurasia. *Nature* **364**, 299–306.

Sengör AMC & Natal'in BA (1996) Paleotectonics of Asia: fragments of synthesis. In: *The Tectonic Evolution of Asia* (eds A. Yin, T.M. Harrison, pp. 486–640. Cambrdige: Cambridge University Press,

Sláma J, Košler J, Condon DJ, Crowley JL, Gerdes A, Hanchar GM, Horstwood Matthew SA, Morris GA, Nasdala L, Norberg N, Schaltegger U, Schoene B, Tubrett MN & Whitehouse MJ (2008) Plešovice zircon — A new natural reference material for U–Pb and Hf isotopic microanalysis. *Chemical Geology* **249**, 1–35.

Soejono I, Buriánek D, Janoušek V, Svojtka M, Čáp P, Erban V & Ganpurev N (2017) A reworked Lake Zone margin: Chronological and geochemical constraints from the Ordovician arc-related basement of the Hovd Zone (western Mongolia): *Lithos*, **294–295**, 112–32.

Soejono I, Buriánek D, Svojtka, M., Žáček, V., Čáp, P. & Janoušek, V. (2016) Mid-Ordovician and Late Devonian magmatism in the Togtokhinshil Complex: new insight into the formation and accretionary evolution of the Lake Zone (western Mongolia) *Journal of Geosciences* (Prague) **61**, 5–23.

Soejono I, Čáp P, Míková J, Janoušek V, Buriánek D, Schulmann K, (2018) Early Palaeozoic sedimentary record and provenance of flysch sequences in the Hovd Zone (western Mongolia): Implications for the geodynamic evolution of the Altai accretionary wedge system. *Gondwana Research* **64**, 163–83.

Sukhbaatar T, Lexa O, Schulmann K, Aguilar C, Štípská P, Wong J, Jiang Y, Míková J & Zhao D (2022) Paleozoic geodynamics and architecture of the southern part of the Mongolian Altai Zone. *Tectonics* **41**, 1–36.

Sun M, Long XP., Cai KD, Jiang YD, Wang B, Yuan C, Zhao GC, Xiao W J & Wu FY (2009) Early Paleozoic ridge subduction in the Chinese Altai: insight from the abrupt change in zircon Hf isotopic compositions. *Science in China Series D: Earth Sciences* **52**, 1345–58.

Sun M, Yuan C, Xiao WJ, Long XP, Xia XP, Zhao GC, Lin S, Wu FY & Kröner A (2008) Zircon U–Pb and Hf isotopic study of gneissic rocks from the Chinese Altai: progressive accretionary history in the early to middle Palaeozoic. *Chemical Geology* **247**, 352–83.

Tomurtogoo, O. (2002) Tectonic map of Mongolia, scale 1:1,000,000 (with Brief Explanatory Notes) (23 p.). Geological Information Centre MRPAM, Ulaanbaatar.

Tomurtogoo O (2006) Tectonic framework of Mongolia. In: D Tomurhuu, BA Natal'in, Y. Ariunchimeg, S. Khishigsuren, G. Erdenesaihan *Structural and Tectonic Correlation across the Central Asian Orogenic Collage: Implications for Continental Growth and Intracontinental Deformation (second international workshop and field excursions for IGC Project 480), abstract and excursion guidebook* (pp. 18–20). Ulaanbaatar: Mongolian University of Science and Technology Press.

Tomurtogoo O (2012) Tectonic subdivision of orogenic belt of Mongolia. Transactions of Institute of Geology and Mineral Resources of MAS, 21, 5–25 (in Mongolian).

Tomurtogoo O (2014) Tectonics of Mongolia. In: Tectonics of Northern, Central and Eastern Asia, explanatory note to the Tectonic map of Northern Central Eastern Asia and adjacent areas at scale 1:2,500,000. 110–126.

Tomurtogoo O (2017) Tectonic subdivision of Mongolia.: scale 1:4,500,000.

Tomurtogoo O, Byamba J, Badarch G, Minjin CH, Orolmaa D, Khosbayar P & Chuluun D (1998) Geological map of Mongolia (scale 1:1,000,000): Ulaanbaatar, Mineral Resources Authority of Mongolia and Mongolian Academy of Sciences.

Tovuudorj D & Sumya T (2008) Geological map of the Western Mongolia, "UGZ-200-II" project: scale 1:200,000.

Wang T, Hong DW, Jahn BM, Tong Y, Wang YB, Han BF & Wang XX (2006) Timing, petrogenesis, and setting of Paleozoic synorogenic intrusions from the Altai Mountains, Northwest China: implications for the tectonic evolution of an accretionary orogen. *Journal of Geology* **114**, 735–51.

Wang YJ, Long XP, Wilde SA, Xu HL, Sun M, Xiao WJ, Yuan C & Cai KD (2014) Provenance of early Paleozoic metasediments in the central Chinese Altai: implications for tectonic affinity of the Altai-Mongolia terrane in the Central Asian Orogenic Belt: *Lithos* **210–211**, 57–68.

Watanabi T, Buslov MM & Koitabashi S (1994) Comparison of arc-trench systems in the Early Paleozoic Gorny Altai and the Mesozoic-Cenozoic of Japan. In: *Reconstruction on the Paleo-Asian Ocean* (ed Coleman, R.G.), pp. 169–90., Utrecht, The Netherlands: VSP.

Wedepohl KH (1995) The composition of the continental crust. *The Journal of the Geochimica et Cosmochimica Acta* **59**, 1217–32.

Williams IS (2001) Response of detrital zircon and monazite, and their U – Pb isotopic systems, to regional metamorphism and host-rock partial melting, Cooma Complex, southeastern Australia. *Australian Journal of Earth Sciences* **48**, 557–80.

Windley BF, Alexeiev D, Xiao W, Kröner A & Badarch G (2007) Tectonic models for accretion of the Central Asian Orogenic Belt. *Journal of the Geological Society of London* **164**, 31–47.

Windley Brian F, Kröner A, Guo J, Qu G, Li Y & Zhang C (2002) Neoproterozoic to Paleozoic Geology of the Altai Orogen, NW China: new zircon age data and tectonic evolution. *The Journal of Geology* **110**, 719–37.

Xia XP, Sun M, Zhao GC & Luo Y (2006a) LA-ICP-MS U-Pb geochronology of detrital zircons from the jining complex, North China craton and its tectonic significance. *Precambrian Research* **144**, 199–212.

Xiao WJ & Kusky TM (2009) Geodynamic processes and metallogenesis of the Central Asian and related orogenic belts: introduction. *Gondwana Research* **16**, 167–69.

Xiao WJ, Windley BF, Han CM, Liu W, Wan B, Zhang JE, Ao SJ, Zhang ZY & Song DF (2018) Late Paleozoic to early Triassic multiple roll-back and oroclinal bending of the Mongolia collage in Central Asia. *Earth-Science Reviews* **186**, 94–128.

Xiao WJ, Windley BF, Sun S, Li JL, Huang BC, Han CM, Yuan C, Sun M & Chen HL (2015) A tale of amalgamation of three Perm-Triassic collage systems in central Asia: Oroclines, sutures, and terminal accretion: *Annual Review of Earth and Planetary Sciences* **43**, 477–507.

Yakubchuk A (2004) Architecture and mineral deposit settings of the Altaid orogenic collage: a revised model. *Journal of Asian Earth Sciences* **23**, 761–79.

Yang TN, Li JY, Zhang J & Hou KJ (2011) The Altai-Mongolia terrane in the Central Asian Orogenic Belt (CAOB): A peri-Gondwana one? Evidence from zircon U–Pb, Hf isotopes and REE abundance. *Precambrian Research* **187**, 79–98.

Yuan C, Sun M, Xiao WJ, Li XH, Chen HL, Lin SF, Xia XP & Long X P (2007) Accretionary orogenesis of the Chinese Altai: insights from Paleozoic granitoids: *Chemical Geology* **242**, 22–39.

Zhang Y, Sun M, Yuan C, Xu Y, Long X, Tomurhuu D, Wang CY, He B (2015e) Magma mixing origin for high Ba–Sr granitic pluton in the Bayankhongor area, Central Mongolia: response to slab roll-back. *Journal of Asian Earth Sciences* **113**, 353–68.

Zonenshain LP (1973) The evolution of Central Asiatic geosynclines through sea-floor spreading. *Tectonophysics* **19**, 213–32.

https://doi.org/10.1017/S0016756824000529 Published online by Cambridge University Press